A second RF-station for ELSA

Jens Derksen

Masterarbeit in Physik
angefertigt im Physikalischen Institut

vorgelegt der
Mathematisch-Naturwissenschaftlichen Fakultät
der
Rheinischen Friedrich-Wilhelms-Universität
Bonn

April 2016

I hereby declare that this thesis was formulated by myself and that no sources or tools other than those cited were used.

Bonn, ...
Date Signature

1. Referee: Priv.-Doz. Dr. Wolfgang Hillert
2. Referee: Prof. Dr. Klaus Desch

Contents

1 Introduction **1**
- 1.1 Motivation . . . 1
- 1.2 Accelerator physics in Bonn . . . 2
- 1.3 Hadron physics . . . 2

2 Particle Accelerators **3**
- 2.1 Particle preparation . . . 3
- 2.2 Particle manipulation . . . 4
- 2.3 Cavities . . . 5
  - 2.3.1 Cavities as resonant circuit . . . 7
- 2.4 Waveguides . . . 9
- 2.5 Klystron . . . 11
- 2.6 Synchrotrons . . . 11
  - 2.6.1 Synchrotron radiation . . . 12
  - 2.6.2 Phase focusing . . . 12
  - 2.6.3 Longitudinal beam dynamics . . . 13
  - 2.6.4 Beam lifetime . . . 14
- 2.7 Magnets . . . 15
  - 2.7.1 Dipole magnets . . . 15
  - 2.7.2 Quadrupole magnets . . . 16

3 Implementation **19**
- 3.1 ELSA . . . 19
- 3.2 Existing RF-Station . . . 19
- 3.3 Additional RF station . . . 22
  - 3.3.1 Cavities . . . 23
  - 3.3.2 Coupling . . . 25
  - 3.3.3 Doorknob-coupler . . . 25
  - 3.3.4 Waveguides . . . 26
  - 3.3.5 Klystron . . . 28
  - 3.3.6 Low level radio frequency signal generation . . . 28

4 Operational interaction of two radio frequency (RF) stations **31**
- 4.1 Second radio frequency station . . . 31
  - 4.1.1 Longitudinal beam dynamics with two RF-stations . . . 31
- 4.2 Software for cavity field parameters . . . 32
- 4.3 Operation without phase difference . . . 34
  - 4.3.1 Efficiency . . . 34

4.3.2 Beam current . . . 36
4.3.3 Synchrotron frequency . . . 36
4.4 Phase stability at injection energy . . . 38
4.5 Operation with phase difference . . . 38
4.6 Coupling factor . . . 39

A Appendix **43**
A.1 Efficiency simulation plots . . . 43
A.2 Mathematical derivations . . . 45
A.2.1 Free field wave equations . . . 45
A.2.2 Modes in cylindrical cavities . . . 46
A.2.3 Longitudinal beam dynamics . . . 47
A.2.4 Large amplitude oscillations . . . 49

Bibliography **51**

List of Figures **53**

List of Tables **55**

Glossary **57**

Acronyms **59**

CHAPTER 1

Introduction

1.1 Motivation

At the electron stretcher accelerator (ELSA), electrons are accelerated to energies of up to 3.2 GeV. This is done by staged acceleration. The last stage is the ELSA stretcherring which can accelerate a beam current of up to 70 mA. A constant beam current of 20 nA can be extracted over a long timescale of up to a minute via resonance extraction. The electrons are used to produce high energetic photons for hadron spectroscopy. In the future processes with small crossections shall be investigated. Therefore the eventrate at the experiment has to be scaled up by one order of magnitude to keep the needed measurement times as short as possible. To provide this eventrate from the accelerator the internal beam current in the stretcherring has also to be scaled up by an order of magnitude to 200 mA. Such high internal beam currents cannot be stored in the stretcherring at this moment: The existing RF station, which has to make the voltage available to accelerate the electrons with needed energy of keV per turn and especially compensate the much more important losses of MeV per turn, the electrons have during the acceleration cycle, is operated at its power limit. The two accelerating cavities which build up the acceleration voltage cannot be provided with more power. Therefore two additional accelerating cavities have to be installed to build up additional acceleration voltage. These cavities will be supplied with RF power by their own amplifier.

During the work of this thesis the preparations to build in these cavities have been accompanied from the physical side of view. The operational interaction of two different accelerating stations has been investigated. Therefore the distribution of acceleration voltages and RF phase have been examined with respect to efficiency, storable beam current and beam quality.

In the beginning of this thesis the basic functional principles of a synchrotron are described to motivate the acceleration with electric RF fields. The focus is on the accelerating cavities of the accelerator in which the accelerating fields are build up and their infrastructure. Additionally longitudinal beam dynamics determined by the RF fields and losses due to synchrotron radiation are discussed. After that the parts which are really used to build up the second accelerating station for ELSA are introduced. The plan for the assembly itself is described and the current status of the conversion is constituted. To get the two seperate accelerating stations working together several parameters can be tuned. The detailed discussion of the settings to get this compound system working together will be declared in the last part of this thesis.

1.2 Accelerator physics in Bonn

In 1952 accelerator physics in Bonn started when Wolfang Paul became university professor at the physics institute. Paul and his team built a 500 MeV synchrotron which is nowadays exhibited in the German Museum Bonn [Hil06a]. A synchrotron is a circular accelerator in which charged particles are accelerated by an radio frequency field and guided on a circular path by magnets. After many diploma and doctoral theses had been written at the synchroton and the technics became outdated, in 1963 the physicists reflected to build a higher energy synchrotron to keep pace with other electron accelerators being build in Hamburg and Cambridge. It became clear that the state government would bear the costs and a 2.5 GeV synchrotron was planned. In 1967 the combined function synchrotron began to operate. Till this day the now called booster synchrotron is running as an injector accelerator at 1.2 GeV for the newest synchrotron build in Bonn called ELSA. The construction of ELSA started in 1982. It was planned to increase the duty factor[1] of the 2.5 GeV synchrotron which was arround 5 %. This factor could be stretched to up to typically 80 %. After ELSA is providing a 3.2 GeV electron beam for hadron physics experiments since 1987 there have been many improvements to the accelerator facility due to the work of junior scientists. Many projects in research of accelerator physics at ELSA[2] continue to be processed. Nowadays the accelerator facility consists of three acceleration stages which are linear accelerator (LINAC), booster synchrotron and ELSA to provide an electron beam up to 3.2 GeV.

1.3 Hadron physics

The accelerated electrons are used for hadron physics experiments. CBELSA [Die+15] and BGO-OD [Sch] are both experiments for meson photoproduction. The extracted electrons from the accelerator radiate high energetic photons in a conversion target by a bremsstrahlungs process. Hence the energy of the scattering electrons can be calculated very precisely from the bending radius of the magnets and the magnetic fieldstrength, the photons energy can be determined from the eletrons remaining energy after conversion. In the detectors these tagged photons scatter on a target, for example liquid hydrogen. In the scattering processes other particles for example bayrons or mesons can be produced which can be detected with the surrounding detector. Measuring production crosssections, quark models can be probed. These measurements give possibilities to understand the strong force which can be described by quantum chromo dynamics (QCD). Therefore the knowledge of the fundamental binding forces can be investigated.

Additionally a direct electron beam can be used for tests of high energy particle detectors. In the near future a centre for detector research and development is being build next to the accelerator facility ELSA, a dedicated beamline for detector research will be in operation [Heu+13].

[1] The duty factor is the ratio between the time where electron beam is available at the experiment and the time of the whole operation cycle which consists of preparation time, energy ramp and extraction duration

[2] ELSA is used as name for the last build synchrotron but sometimes also for the accelerator facility in Bonn as a whole

CHAPTER 2

Particle Accelerators

To understand how charged particles are prepared for the experiments and accelerated to the desired energies at first the main concepts and components of particle accelerators will be described. Particle preparation, acceleration and guiding will be covered. In a circular accelerator longitudinal particle motion and interaction with alternating accelerating fields are described.

Since the thesis is about an additional station to build up extra accelerating voltage, the focus will be on RF-systems for particle accelerators especially for synchrotrons.

2.1 Particle preparation

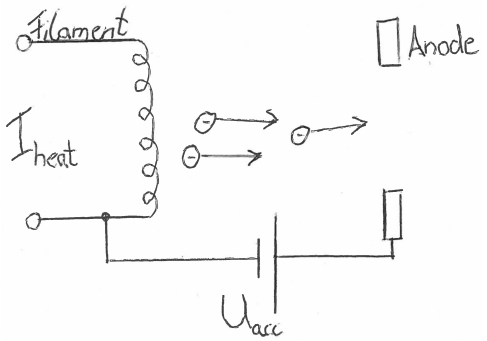

Figure 2.1 – Sketch of a thermionic electron gun

In order to accelerate a particle beam consisting of electrons at first free, unbound electrons have to be prepared. The easiest way to produce thermionic electrons is to heat a filament by applying an electric heating current I_{heat} shown in figure 2.1 . Due to this heating of the kathode material, free elctrons are generated by thermionic emission. The electrons kinetic energy overcomes the work function of the material and they get free. If one applies a potential U_{acc} between this kathode and an anode, the electrons will be accelerated out of the filament towards the anode. The same technique of electron production was used in television tubes. Typical potentials in these electron sources for accelerators are 50 kV to 150 kV.

2.2 Particle manipulation

After being prepared the electrons can be manipulated by electric $\vec{E}$ and magnetic $\vec{B}$ fields. The force which acts on the particles is the Lorentz force $\vec{F_L}$:

$$\vec{F_L} = q\left(\vec{E} + \vec{v} \times \vec{B}\right) \tag{2.1}$$

Where q and $\vec{v}$ are the charge and velocity of the particle. Hence the force of the magnetic field is always perpendicular to the particles velocity and its strength will grow with higher particle velocities, it is used to guide the particle beam, electric fields have to be used to increase the particles energy.

Static acceleration

If a particle traverses an electric field E of length L it gains the kinetic energy ΔE_{kin}.

$$\Delta E_{\text{kin}} = q \int_0^L \left|\vec{E}\right| \, \mathrm{d}z = q \cdot U \tag{2.2}$$

U is the potential between 0 and L. The first static acceleration is applied directly after production of the electrons. The particle passes the potential U_{acc} between the kathode and the anode of the source. After the source, at the entrance of the next stage of acceleration the electrons have the kinetic energy of approximately 50 keV.

Since the energies one wants to obtain for the experiments are in the region of GeV one has to apply a voltage of GV to the electrons. Voltages of this magnitude can not be produced by use of a static electric fields due to the electrical breakdown voltage of vacuum. To avoid sparkovers one does not use static but alternating electric fields in the radio frequency regime.

Acceleration with radio frequency fields

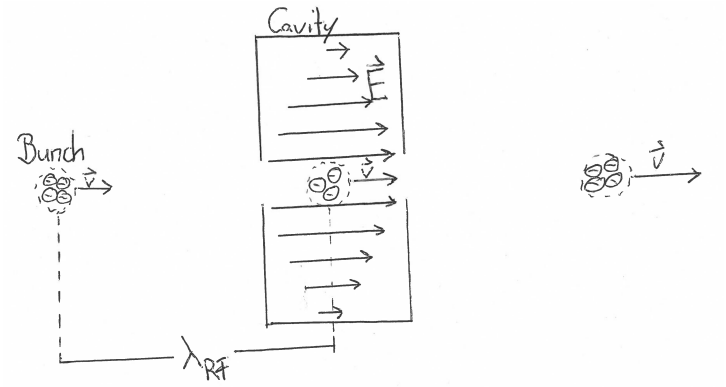

Figure 2.2 – RF acceleration of a bunched electron beam

Since the alternating electric fields used for particle acceleration have frequencies f_{RF} in the radio region they are called RF-fields. In contrast to the electrostatic acceleration with continuous beam, RF-accelerators have to use a bunched beam. This is because of the electric field $\vec{E}$ used for acceleration half of the period time points towards the electrons propagation direction and velocity $\vec{v}$. The electrons would lose energy if they would pass the cavity in this timeslot. Particles can only be accelerated, if

they pass the electric field when it points in their own propagation direction, that is the direction of their momentum vector $\vec{p} = m\vec{v}$ where m is the mass of the particles (see figure 2.2). The bunches of particles have to be separated by the wavelength λ_{RF} of the used RF-field $\lambda_{\mathrm{RF}} = {}^{c}/_{f_{\mathrm{RF}}}$ where c is the velocity of light.

2.3 Cavities

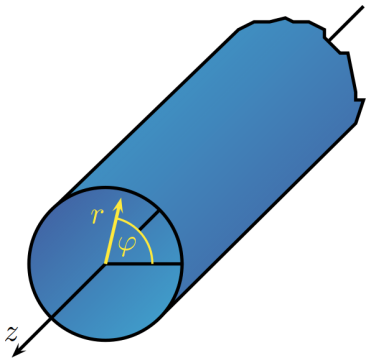

Figure 2.3 – Coordinate system used to describe cylindrical resonators [Heu11]

Cavities are hollows surrounded by conducting walls. In accelerator physics cylindrical cavities are used to build up high alternating electric fields with voltages of some MV. To learn which fields can be build up in such structures the free field wave equations 2.3 and 2.4 for the electric field $\vec{E}$ and magnetic field $\vec{B}$ can be solved (for derivation of the wave equations see appendix A.2).

$$\Delta\vec{E} - \frac{1}{c^2}\frac{\partial^2\vec{E}}{\partial t^2} = 0 \tag{2.3}$$

$$\Delta\vec{B} - \frac{1}{c^2}\frac{\partial^2\vec{B}}{\partial t^2} = 0 \tag{2.4}$$

Solving these equations for the boundary conditions of a pure cylindrical so called pillbox cavity in cylindrical coordinates (shown in figure 2.3) leads to solutions with different field configurations called modes, depending on the geometry of the cavity with radius R and length L. The resonators consist of conducting walls therefore the transverse electric and parallel magnetic components of the fields have to vanish at the surface. One has to distinguish between transversal magnetic TM_{mnp} modes with no longitudinal magnetic and transversal electric TE_{mnp} modes with no longitudinal electric field. The indices m,n and p characterize the field distribution. m is equal to the number of periodes in φ direction, n the number of knots in r direction and p the number of half periodes in z direction. Since in an accelerator one wants to use longitudinal electric fields to accelerate the electrons, TM_{mnp} modes are used. (The complete mathematical description of the fields for both TE and TM modes can be found in appendix A.2.2).

For the electric field E_z in direction of motion of the electrons z for the TM_{mnp} modes, one gets:

$$E_z = E_0 J_m\left(\frac{x_{mn}r}{R}\right)\cos(m\varphi)\cos\left(\frac{p\pi z}{L}\right)e^{i\omega_{mnp}t} \tag{2.5}$$

$J_m(x)$ is the Bessel function of m-th order and x_{mn} is the n-th zero of the Bessel function of m-th order.

The oscillation frequencies f_{mnp} for the TM_{mnp} modes can be written as

$$f_{mnp} = \frac{c}{2\pi}\sqrt{\left(\frac{x_{mn}}{R}\right)^2 + \left(\frac{p\pi}{L}\right)^2}. \tag{2.6}$$

The most important mode for particle acceleration is the TM_{010} mode which has the largest longitudinal electric field on the z-axis (A simulation of the E and B fields can be seen in figure 2.4).

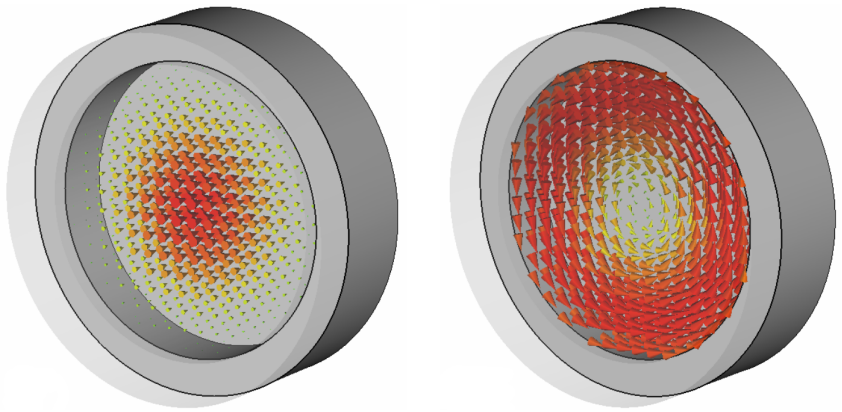

Figure 2.4 – Simulation of the E (left) and B field (right) of the TM_{010} mode in a pillbox cavity simulated with *CST Microwave studio*. The higher the field strength the bigger the arrows. Additionally higher field strength are shown in red lower in yellow. [Hil08]

For this mode the electric field on the axis ($r = 0$) in a pillbox cavity becomes:

$$\vec{E} = E_0 e^{i\omega_{mnp}t}\vec{e}_z \tag{2.7}$$

Where $\vec{e}_z$ is the unit vector in z direction, what means the field is pure longitudinal. The fieldstrength only changes with time. From the electrical field in the cavity the accelerating voltage U_0 can be calculated.

$$U_0 = \int_0^L |\vec{E_0}(z)|\,\mathrm{d}z \tag{2.8}$$

Since the electric fields change with time, also the accelerating voltage does. Therefore the voltage can

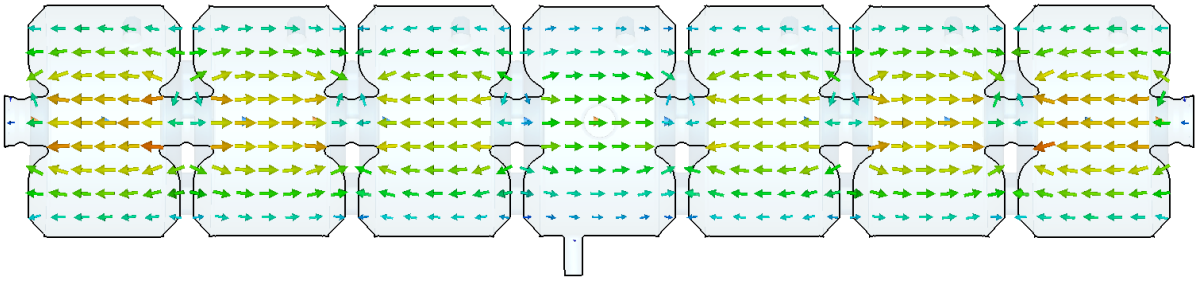

Figure 2.5 – Simulation of the electric field of the TM_{010} mode in a seven cell positron electron tandem ring accelerator (PETRA) type cavity. The higher the fieldstregth the bigger the arrows (for high fieldstrength yellow/orange and lower blue). The nosecones which enhance the fieldstrength on the beam axis can be seen, too. Fields are calculated numerically with *CST Microwave Studio*

be written dependent of t and with an additional phase ϕ:

$$U = U_0 \cdot \sin(\omega_{\mathrm{mnp}} t + \phi) \tag{2.9}$$

The electrons need some time to pass through the cavity while the field is changing. Therefore the voltage which accelerats the electrons has to be weighted with the transition time factor Λ to get the effective acceleration voltage $U_0^{\mathrm{eff}} = \Lambda \cdot U_0$. The transition time factor due to the changing field can be written as [Lee12]:

$$\Lambda = \left| \frac{\int_0^L \left| \overrightarrow{E_0}(z) \sin\left(\frac{\omega_{mnp}}{c} z + \phi\right) \right| \mathrm{d}z}{\int_0^L \left| \overrightarrow{E_0}(z) \right| \mathrm{d}z} \right| \tag{2.10}$$

Cavities in particle accelerators cannot be pure pillbox cavities. The used cavities have holes in their walls so that the particle beam can traverse it. Moreover nosecones were developed to enhance the fieldstrength on the beam axis and get a higher acceleration voltages. Fields in such cavities with such complicated geometries cannot be solved mathematically. The fields can only be simulated with numerical methods or be measured (Chapter 3.3.1). A simulation of the electric field in a PETRA type seven cell cavity which will be used for the new RF-station can be seen in figure 2.5.

2.3.1 Cavities as resonant circuit

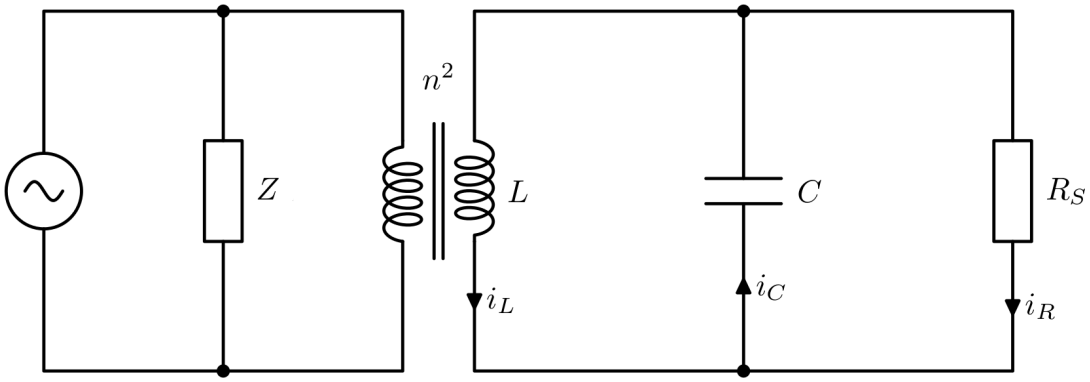

Figure 2.6 – Equivalent circuit of a cavity with RF generator and coupling [Sch15]

The properties of cavities can be described with an *LRC* equivalent circuit. Near a resonance a RF resonator behaves like an damped *LC* oscillation circuit. The resonance frequency ω_0 of the oscillation circuit is:

$$\omega_0 = \frac{1}{\sqrt{LC}} \tag{2.11}$$

Inductance L and Capacitance C can be varied by the geometry of the cavity as described in the equations 2.5 and 2.6. The walls of the cavity behave like the inductance in the equivalent circuit and the build up field in the cavity like the field in a capacitor. Balancing currents flew through the walls of the resonator. As a measure for the performance of the resonator the unloaded quality factor Q_0 can be

indicated [Wil92].

$$Q_0 = \frac{\omega_0 W}{P} \tag{2.12}$$

It is propotional to the ratio of the stored energy in the cavity W and the dissipated power in the walls P and therefore a measure how good energy can be stored in the cavity. The complex impedance of the cavity can be written as Z_C, with R_s the so called shunt impedance of the cavity (see figure 2.6).

$$Z_C(\omega) = \frac{R_s}{1 - iQ\left(\frac{\omega_0}{\omega} - \frac{\omega}{\omega_0}\right)} \tag{2.13}$$

In case of resonance $\omega = \omega_0$ this impedance becomes real $Z_C(\omega_0) = R_s$. We want to couple in all the power of the generator (on the left in the figure 2.6) into the cavity. Therefore the impedance of the generator Z and the impedance of the cavity have to be matched. Electro magnetic signals can be coupled into a cavity in different ways: For example the pin coupling with a pin in the wall of the resonator which couples to the electric fields or a loop which couples to the magnetic fields like a transformer. The coupler is a connection between the middle conductor of a coaxial cable and the wall of the cavity and therefore builds one loop. By changing of the geometry of this coupler the coupling n between the transmission line and the cavity can be adjusted. In the case the coupling factor

$$\kappa = \frac{n^2 Z}{R_s} \tag{2.14}$$

becomes one the coupling is called critical. For this coupling all the power P is coupled in the cavity and converted into the electric field. The peak voltage U in the cavity can be written as:

$$U = \sqrt{2PR_s} \tag{2.15}$$

The required unloaded input power is defined as

$$P = \frac{U^2}{2R_s}. \tag{2.16}$$

If a bunched beam passes the cavity it acts like an additional load for the generator. In this case the needed power of the generator can be written as the sum of the power which is needed only to build up the field and the power which is needed due to beamloading [Wil92].

$$P = \frac{U^2}{2R_s} + U \sin(\phi_0) I_{\text{beam}} \tag{2.17}$$

Here I_{beam} is the beam current of the charged particles and $U \sin(\phi_0)$ the voltage in the cavity when the particle passes through it. In this case the coupling factor also changes due to the additional load. To get no reflections at the coupling with beam loding the optimum coupling factor can be written as [Rot08]:

$$\kappa_{\text{opt}} = 1 + \frac{P_{\text{beam}}}{P_{\text{field}}} \tag{2.18}$$

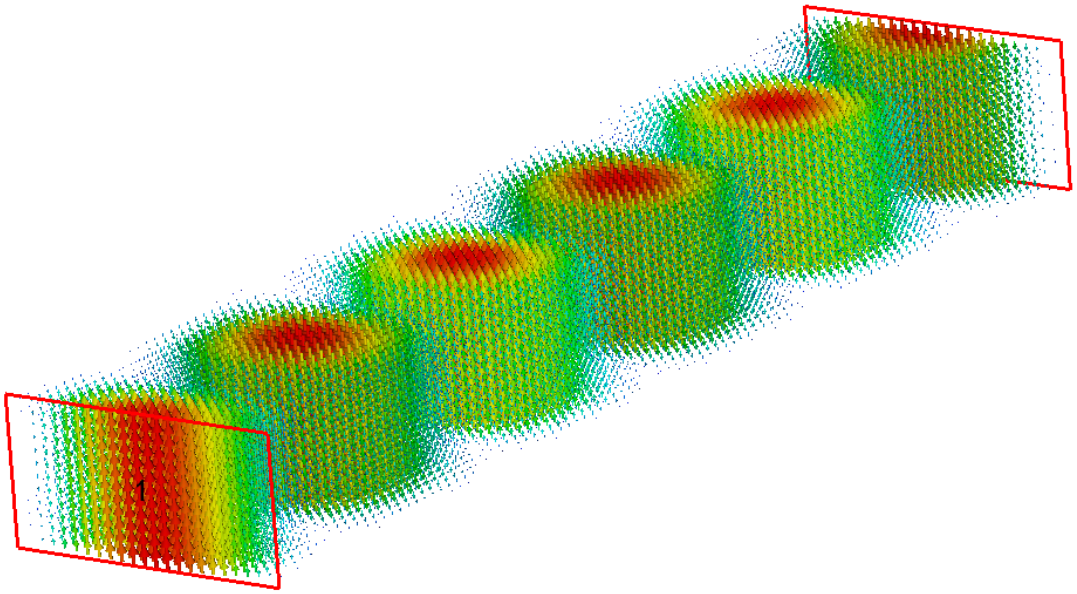

Figure 2.7 – Wave progatation of the TE_{10}-mode through a WR1800 waveguide simulated with *CST Microwave studio*. The electric field strength is depicted. Higher field strength are red, lower blue. The picture is a snapshot of the fields. The 500 MHz wave is injected at the left end of the waveguide and propagates to the other end. The right end of the waveguide simulates an matched termination, that the waves are not reflected back in the waveguide.

2.4 Waveguides

As in the cavities the electric fields in the waveguides can be described by the wave equations 2.3 and 2.4. If these are solved for the boundary conditions of conducting surfaces of a rectangular waveguide with width a and height b, TM- and TE-modes occur. For the TM_{mn}-modes one gets [Jac75]:

$$E_z = E_0 \sin\left(\frac{\pi m}{a}x\right)\sin\left(\frac{\pi n}{b}y\right)e^{i(\omega t - k_z z)} \tag{2.19}$$

$$H_z = 0 \tag{2.20}$$

While the TE_{mn}-modes can be described as follows.

$$H_z = H_0 \cos\left(\frac{\pi m}{a}x\right)\cos\left(\frac{\pi n}{b}y\right)e^{i(\omega t - k_z z)} \tag{2.21}$$

$$E_z = 0 \tag{2.22}$$

To get these waves travelling through the waveguide the exponent $(\omega t - k_z z)$ has to be real. One gets a critical wave number k_c, this is the smallest wave number for which the waves travel through the waveguide and are not exponentially damped. It is also called cutoff wavenumber:

$$k_c^2 = \frac{\omega^2}{c^2} - k_z^2 \tag{2.23}$$

This cutoff wavenumber can be determined from the geometry of the waveguide and modenumbers:

$$k_c = \sqrt{\left(\frac{\pi m}{a}\right)^2 + \left(\frac{\pi n}{p}\right)^2} \tag{2.24}$$

With $k_c = \omega_c/c = 2\pi f_c/c$ the cutoff frequency f_c can be written as:

$$f_c = \sqrt{\left(\frac{mc}{2a}\right)^2 + \left(\frac{nc}{2b}\right)^2} \tag{2.25}$$

Electromagnetic waves with lower frequencies than this frequency do not propagate through the waveguide. In the accelerator waveguides are used to transmit the RF power from the generator to the cavities by the TE_{10} mode, since suitable coaxial cables would have higher losses at the used powers and frequencies in contrast to waveguides.

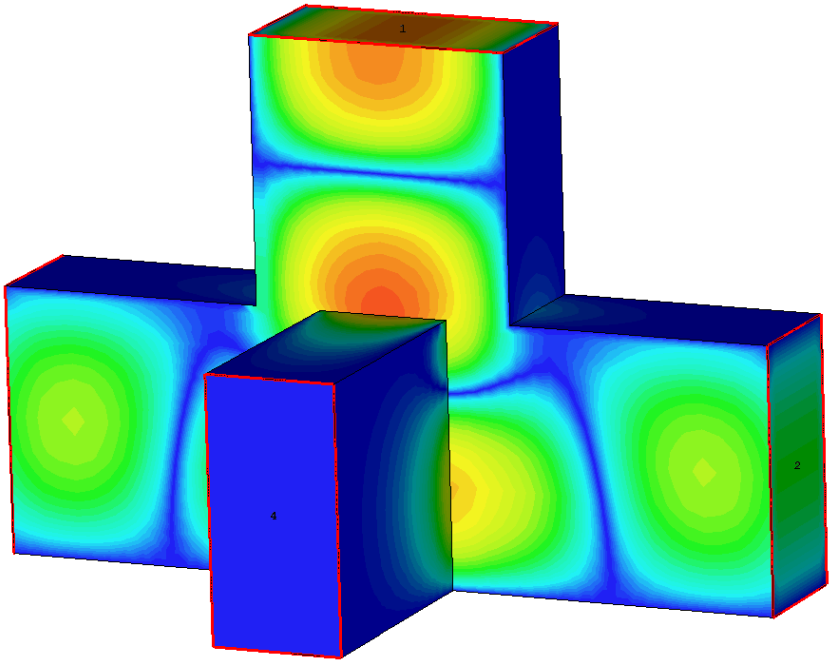

Figure 2.8 – Electric fields of the TE_{10} mode with a frequency of 500 MHz in a magic T with RF power injected from the top and the fourth port in the front terminated with the impedance of the waveguide. Higher field strength are depicted in red, lower in blue.The fields are calculated with *CST Microwave studio*.

A magic T is a waveguide four port (Figure 2.8). If one port of a magic T is terminated, a signal which is injected in one port is divided with equal powers to the two other ports. In this way magic Ts are often used to split up the power of one generator for two cavities.

Another waveguide multiport, used at particle accelerators is the circulator (Figure 2.9). A circulator is a three port which passes the power to the next port. But only in one direction. A signal coming in at port one is passed to port two. From two, the signals are passed to three. And from three to one. This can be used to create a waveguide diode. If the signal is terminated for example by a water cooled load at port three. Only signals from port one to two will propagate through an adjoining waveguide system. If a electromagnetic wave is reflected back into the circulator, it will be terminated in the load. Therefore circulators are used in waveguide systems to protect sensible RF components from reflected power.

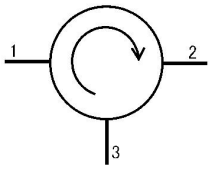

Figure 2.9 – Scheme of a circulator

2.5 Klystron

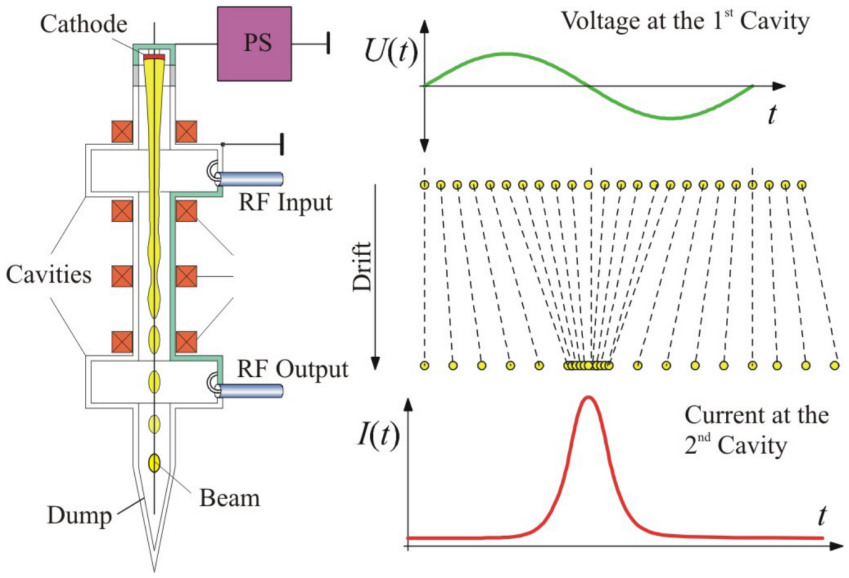

Figure 2.10 – Working principle of a klystron [Hil06a].

A klystron is a RF-amplifier. Its functional principle can be seen in figure 2.10. At the top of the klystron at the cathode a continuous electron beam is produced and accelerated by the voltage provided by the power supply (PS). In the first cavity the low level RF signal is fed in, so that some electrons of the continuous beam are accelerated further and other are decelerated, since they traverse the cavity at different voltages. This leads to a bunching of the beam during the drift space. The second cavity is passed by the high intesity bunches of electrons with a distance of the RF-wavelength. In the second cavity this bunches excite a RF oscillation with high field strength. Therefore a high power RF signal can be coupled out of the second cavity.

2.6 Synchrotrons

Since one wants to use the same acceleration cavity (pink in figure 2.11) for many times, the electrons have to be bend on a circular path, therefore the homogeneous magnetic field of dipole magnets is used (section 2.7.1). Quadrupole magnets are used to focus the particle beam (section 2.7.2). Bending charged particles trajectories on circular path has the advantage to use the same cavities for many times but comes also with disadvantages such as synchrotron radiation mentioned in the next chapter.

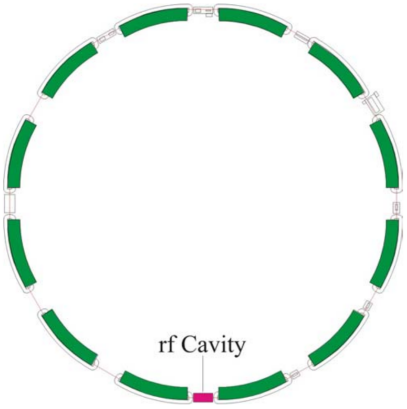

Figure 2.11 – Scheme of a circularly shaped synchrotron. The dipole magnets bending the beam on a circular path are shown in green. The RF-section is depicted in pink.

2.6.1 Synchrotron radiation

If the momentum p of charged particles is changed, electromagnetic waves are emitted. The bending onto the circular trajectory in the dipole magnets of a synchrotron is such a change of the momentum of the electrons. Therefore the radiated power P_{rad} can be described as follows [Wil92]:

$$P_{\mathrm{rad}} = \frac{q^2 c \gamma^2}{6\pi\varepsilon_0 (m_0 c^2)^2} \left(\frac{\mathrm{d}p}{\mathrm{d}t}\right)^2 \tag{2.26}$$

With the lorentz-factor $\gamma = (1-\beta^2)^{-1/2}$ with $\beta = v/c$, ε_0 is the vacuum permittivity and m_0 is the rest mass of the charged particle. For electrons with velocities $v \ll c$ this radiated power is ignorable, but if the velocities are in the same order as the speed of light c, as it is in a GeV electron accelerator, the radiated power becomes relevant. In an electron accelerator the energyloss per turn ΔE_{rev} is of importance. Therefore it can be described by the particles energy E and the bending radius of the dipole magnets R:

$$\Delta E_{\mathrm{rev}} = \frac{e^2\beta^3\gamma^4}{3\varepsilon_0 R} = \frac{e^2\beta^3}{3\varepsilon_0 \left(m_o c^2\right)^4} \frac{E^4}{R} = W(E) \tag{2.27}$$

The voltage, which is needed in the cavity to compensate these losses, is called circumference voltage U_{rev}:

$$U_{\mathrm{rev}} = \frac{\Delta E_{\mathrm{rev}}}{e} = \frac{W(E)}{e} \tag{2.28}$$

A particle, with its synchrotron radiation losses exactly compensated by the acceleration on reference phase ϕ_0 in the cavity, is called reference particle:

$$U_{\mathrm{rev}} = U_0 \sin(\phi_0) \tag{2.29}$$

2.6.2 Phase focusing

Since the emission of synchrotron radiation is a statistical process, a distribution of the particle momenta around the reference momentum p_0 exists. Electrons with slightly differing momentum $p = p_0 + \Delta p$ to

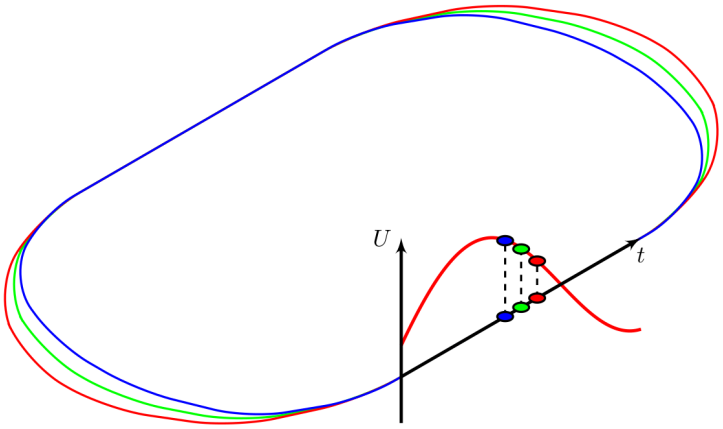

Figure 2.12 – Principle of phase focusing in an elliptical accelerator [Sch15]

the momentum of the reference particle p_0 are bend by the dipole magnets differently. Since the magnetic field in the dipoles is constant, electrons with different momenta are bend with different bending radii (see figure 2.12 and equation 2.40). Electrons with a slightly higher momentum are deflected less in the dipole magnets. They take a little longer path $L = L_0 + \Delta L$ (equation 2.30) through the circular accelerator (red particle in figure 2.12) and need more time $T = T_0 + \Delta T$ (equation 2.31) to come back to the accelerating structures as the reference particle with pathlength L_0 and revolution time T_0.

$$\frac{\Delta L}{L_0} = \alpha_c \frac{\Delta p}{p_0} \tag{2.30}$$

$$\frac{\Delta T}{T_0} = -\eta \frac{\Delta p}{p_0} \tag{2.31}$$

The factor α_c, which connects the relative momentum spread with the variation of the pathlength, is called momentum compaction factor and is only dependent on the magnetic structure of the accelerator. $\eta = 1/\gamma^2 - \alpha_c$ is called the slip factor [Wie93]. For ELSA the measured momentum compaction factor is $\alpha_c = 0.0601 \pm 0.0002$ [Sch+15a].

If the electron needs more time for a revolution, it passes the accelerating structure later on another phase $\phi = \phi_0 + \Delta\phi$ and the accelerating field has reduced with respect to the reference particle. In the next turn for this electron the process is inverted. It has less energy gain, needs less time and in the next acceleration process gains more energy than the reference particle (blue particle in figure 2.12). This leads to an oscillation around the reference phase which is called synchrotron oscillation.

2.6.3 Longitudinal beam dynamics

The synchrotron oscillations of the particles around the reference phase ϕ_0 (green particle in figure 2.13) can be described with the following equation of motion (for derivation, see appendix A.2.3).

$$\frac{\mathrm{d}^2\Delta\phi}{\mathrm{d}t^2} + 2\alpha_s \frac{\mathrm{d}\Delta\phi}{\mathrm{d}t} + \Omega_s^2 \Delta\phi = 0 \tag{2.32}$$

The frequency of this oscillation called synchrotron frequency is $f_s = \Omega_s/2\pi$ and the damping α_s can be described with a damping time $\tau_s = \alpha_s^{-1}$. α_s is only dependent on the synchrotron radiation losses of the particles. The synchrotron frequency f_s for particles circulating in an accelerator with acceleration

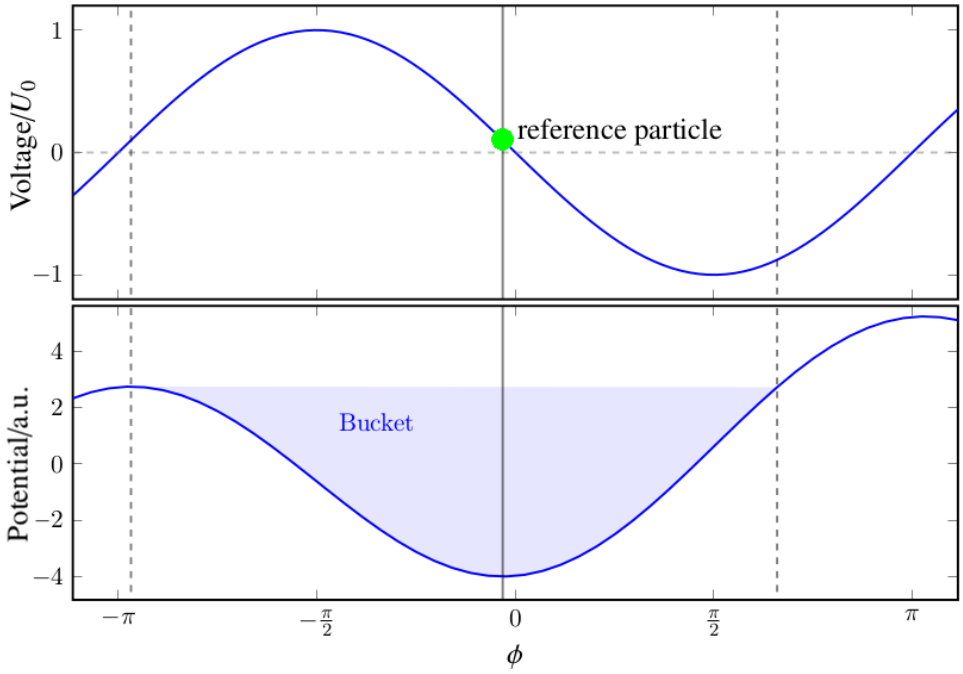

Figure 2.13 – Acceleration voltage and potential dependent on phase ϕ of the accelerating voltage [Sch15].

voltage $U(\phi) = U_0 \sin(\phi)$ can be written as (Equation A.26 in the appendix):

$$f_s = \sqrt{\frac{h\eta e}{2\pi\beta^2 T_0^2 E_0} U_0 \cos(\phi_0)} \tag{2.33}$$

The particles oscillate in the RF-potential which has the following form (for derivation, see appendix A.2.4):

$$V(\Delta\phi) = -\frac{e\beta^2 E_0 U_0}{\pi h\eta}\Big(\cos(\phi_0 + \Delta\phi) + \Delta\phi \sin(\phi_0)\Big) \tag{2.34}$$

The form of the potential can be seen in figure 2.13. The stable region in the potential in which the electrons can oscillate, between the dashed lines, is called bucket. In every bucket in the accelerator a bunch of electrons can be placed. The number of buckets is the harmonic number $h = \frac{\omega_{RF}}{\omega_0}$, which is 274 for ELSA.

2.6.4 Beam lifetime

The beam lifetime is dependend on the slope of the RF voltage or the depth of the RF-potential. One can influence the depth of the potential by using a higher peak voltage with respect to the voltage on reference phase. This is called overvoltage factor q:

$$q = \frac{U_0}{U_0 \sin(\phi_0)} \tag{2.35}$$

An higher overvoltage factor q associates with an higher synchrotron frequency f_s due to equation 2.33. The beam lifetime χ_s can be written as (taken from [Lee12]):

$$\chi_s = \tau_s \cdot \frac{e^{\frac{\xi_s}{2}}}{\xi_s} \tag{2.36}$$

With

$$\xi_s = C(E_0) \cdot \underbrace{2\left(\sqrt{q^2-1} - \arccos\left(\frac{1}{q}\right)\right)}_{F(q)} \tag{2.37}$$

$C(E_0)$ is a constant which depends on the energy of the beam and the magnetic structure of the accelerator. $F(q)$ is called energy aperture function, it is increasing for $q > 1$ and proportional to q for $q \gg 1$. This means the beam lifetime χ_s grows with the overvoltage factor q, since q is always bigger than one.

2.7 Magnets

2.7.1 Dipole magnets

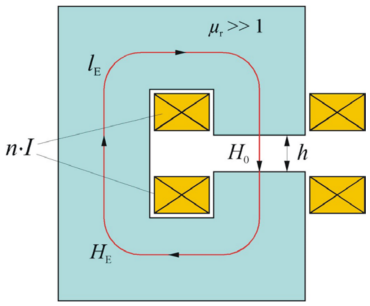

Figure 2.14 – Sketch of a C-shaped electric dipole magnet [Hil06b].

According to the Lorentz-force (Equation 2.1) $\vec{B}$-fields cause a force perpendicular to the velocity $\vec{v}$ of the particles. Dipole magnets (Figure 2.14) have a homogeneous field in the region of the beam axis. The needed strength of the magnetic field for a given bending radius R can easily be calculated from the equality of Lorentz- and centrifugal force:

$$F_L = F_c \tag{2.38}$$

$$\Leftrightarrow q \cdot (v \cdot B) = \frac{mv^2}{R} \tag{2.39}$$

$$\Leftrightarrow B = \frac{mv}{qR} = \frac{p}{qR} = \frac{p}{q}\kappa \tag{2.40}$$

Electric magnets are used to adjust the magnetic field to the raising particle momentum p, since the radius has to be constant to keep the particles in the accelerator. Therefore the magnetic field strength can be expressed in terms of winding number n, current I and gap height h:

$$\kappa = \frac{1}{R} = \frac{e}{p}B = \frac{e}{p}\frac{\mu_0 n \cdot I}{h} \tag{2.41}$$

Here e is the elementary charge and μ_0 the magnetic permeability.

2.7.2 Quadrupole magnets

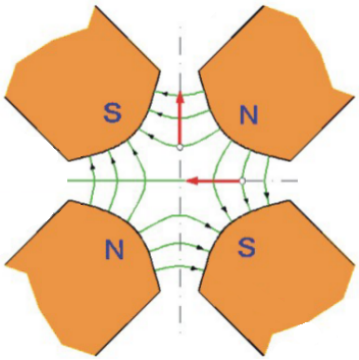

Figure 2.15 – Sketch of a quadrupole magnet, the hyperbolic shaped poles are orange. The magnetic field lines are depicted in green, while the forces on two particles with different positions on the quadrupole are shown in red. [Hil06b].

The bunches in the accelerator consist of many equally charged particles which repel each other and the trajectories of the particles are not exactly parallel. Because the beam has only limited space in the vaccum chamber, one has to focus the particle beam. To focus particles with different transverse distances from the beam axis on the same focal point, one needs a restoring force which increases linearly with the distance from the beam axis. Such a force can be provided by quadrupole magnets with hyperbolic pole pieces (figure 2.15). For those magnets the characterising quantity is the quadrupole strenght k.

$$k = \frac{e}{p}\frac{2\mu_0 n \cdot I}{a^2} \tag{2.42}$$

Where a is the shortest distance between beam axis and the poles of the quadrupole. With the quadrupole strength k and the length of the quadrupolefield L a focal length f of the quadrupole can be defined.

$$f = \frac{1}{k \cdot L} \tag{2.43}$$

Quadrupole magnets have one disadvantage. A charged beam is focused in one plane but defocused in the other. This can be seen in figure 2.15, since the force on one particle (red) points to the center of the quadrupole but on the particle in the other plane it points outwards. Using a focusing $f_1 = f$ and a defocusing $f_2 = -f$ magnet behind each other an overall focusing f_{tot} can be achieved. As one knows from optics the total focal length f_{tot} of a system of two thin lenses can be described as follows, where d is the distance between these lenses:

$$\frac{1}{f_{tot}} = \frac{1}{f_1} + \frac{1}{f_2} - \frac{d}{f_1 \cdot f_2} \tag{2.44}$$

$$\Rightarrow \frac{1}{f_{tot}} = \frac{1}{f} - \frac{1}{f} + \frac{d}{2 \cdot f} = \frac{d}{2 \cdot f} \tag{2.45}$$

$$\Rightarrow f_{tot} = \frac{2 \cdot f}{d} \tag{2.46}$$

Since one uses a focusing magnet (F), then driftspace where no magnet and no focusing is present (0 or

O) and a defocusing magnet (D) this pattern of magnets is called FODO-lattice. Another approach is to use so called combined function magnets, which have no pure dipole field but the poles are tilted in such a way, that the fields have an amount of quadrupole fields. Combined function magnets at ELSA are used in the booster synchrotron.

CHAPTER 3

Implementation

3.1 ELSA

ELSA is an electron accelerator with three accelerating stages (shown in 3.1). Either thermionic or spin polarized electrons can be accelerated. In the first stage electrons are accelerated by one of the two LINACs to be filled in the booster synchrotron. In the booster synchrotron build by Wolfgang Paul and his team (see section 1.2) the electron energy can nowadays be increased up to 1.6 GeV. In normal operation the energy is increased to 1.2 GeV to transfer the electrons into the ELSA stretcherring. In the stretcherring the electrons can be stored. In normal mode of operation, the so called booster mode, electrons are accumlated in the stretcherring, then the energy is ramped to extraction energy between 0.5 GeV to 3.2 GeV to extract them to one of the hadron physics experiments CBELSA or BGO-OD for approximately four seconds to one minute (the progression of beam current and energy in the boostermode can be seen in figure 3.2).

3.2 Existing RF-Station

The existing RF-station of the strecherring consits of two normal conducting PETRA five cell cavities from DESY [DES10]. The main parameters for this type of cavities are summed up in table 3.1. The

TM_{010} mode frequency @40 °C	499.67 MHz
Unloaded quality factor Q_0	29 500
Shunt impedance R_s	15 MΩ
Detuning due to temperature	8 kHz °C^{-1}
Nominal accelerating voltage	1.09 MV

Table 3.1 – Parameters of PETRA five cell cavities as specified in the data sheet [DES10]

RF-power is generated by a Thomson-CSF F2055 Klystron [Tho81]. After generation the power is transmitted to the cavities by WR-1800 waveguides [DES05] and divided in two equal parts by a magic T. The halved power is then coupled into the cavities by use of a doorknob coupler [DESa] and a cavity input coupling loop [DES11]. A doorknob coulper is a adapter for RF-waves to match the rectangular shape of the WR1800 waveguides with the coaxial shape of the coupling loop. The peak accelerating voltage U_{cav}

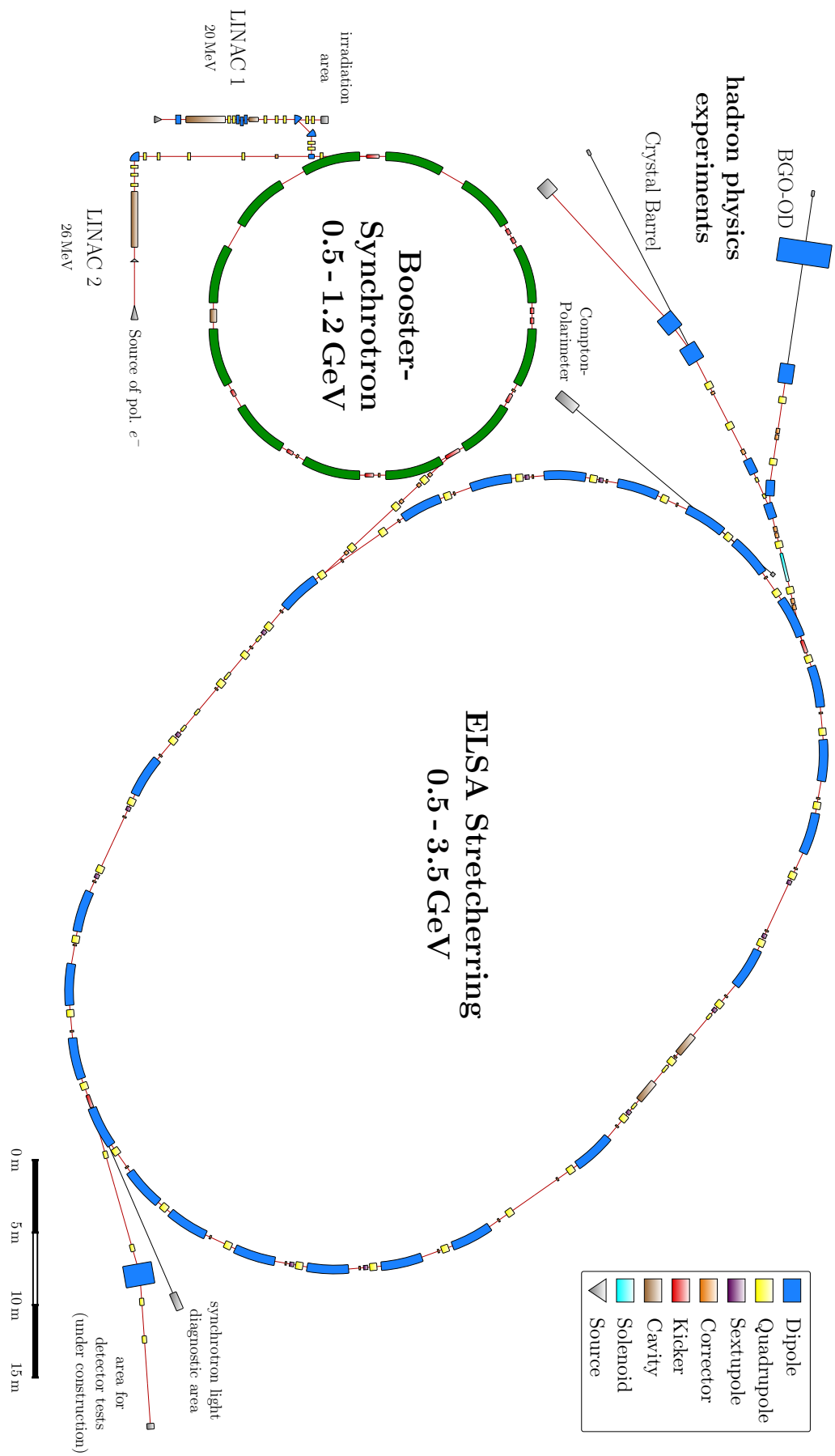

Figure 3.1 – ELSA floorplan

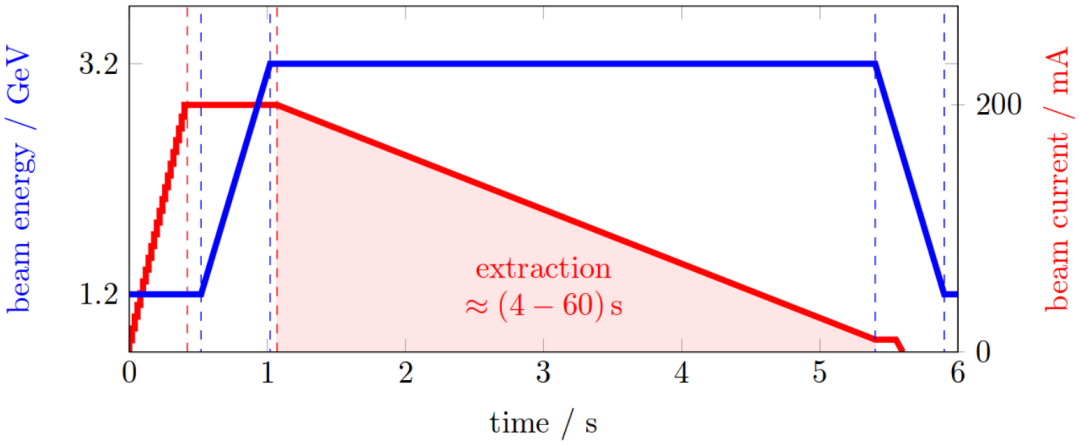

Figure 3.2 – Beam current and energy in the boostermode of ELSA [Sch+15b]

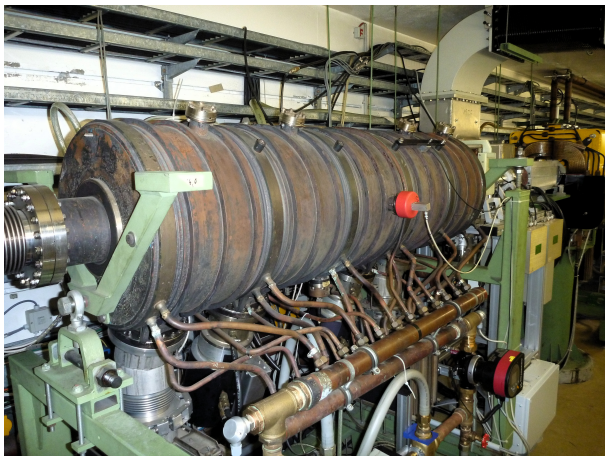

Figure 3.3 – Photograph of one PETRA five cell cavity in the existing RF station.

can be calculated via incoupled power P_{field} and shuntimpedance of the cavity R_s (Section 2.3.1).

$$P_{\text{field}} = \frac{U_{\text{cav}}^2}{2R_s} \tag{3.1}$$

In the existing RF-station the two cavities are aligned in a way that their two middle cells have a distance of an integer multiple of the RF wavelength $\lambda_{\text{RF}} = \frac{c}{f_{\text{RF}}} \approx 60\,\text{cm}$. Therefore their accelerating voltages can be summed together. To get the RF power coupled in the cavities on the same phase, the magic T has to be aligned exactly in the middle between the cavities, hence both arms from the magic T to the doorknob couplers have to have the same length to get the same phase of the RF incoupled in both cavities. This alignment was achieved by an experimental method described in [Sch15, pp.124ff]. Because the electrons will pass both cavities on the same phase ϕ, the accelerating voltage can be written as:

$$U_1(\phi) = 2 \cdot U_{\text{cav}} \sin(\phi) \tag{3.2}$$

The power requirement of the existing accelerating section depends on the power needed due to beam loading P_{beam} and the power which is needed to build up the field in the cavities P_{field} (see chapter 2.3.1).

Since the two cavities are supplied by one klystron one gets for the needed power P_1:

$$P_1 = P_{\text{beam}} + 2P_{\text{field}} \tag{3.3}$$

$$= U_1(\phi_0) \cdot I_{\text{beam}} + 2\frac{U_{\text{cav}}^2}{2R_s} \tag{3.4}$$

$$= 2U_{\text{cav}} \sin(\phi_0) \cdot I_{\text{beam}} + \frac{U_{\text{cav}}^2}{R_s} \tag{3.5}$$

With $2U_{\text{cav}} \sin(\phi_0) = U_{\text{rev}}(E_0)$ and $U_0/2 = U_{\text{cav}}$ one gets for the beam current:

$$I_{\text{beam}} = \left(P_1 - \frac{U_0^2(f_s)}{4R_{1,s}} \right) \frac{1}{U_{\text{rev}}(E_0)} \tag{3.6}$$

With the maximum power of 200 kW the klystron can deliver, the highest achievable beam current is 70 mA at an energy of 3.2 GeV. This means additional beam power is needed to allocate the requested internal beam current of 200 mA.

3.3 Additional RF station

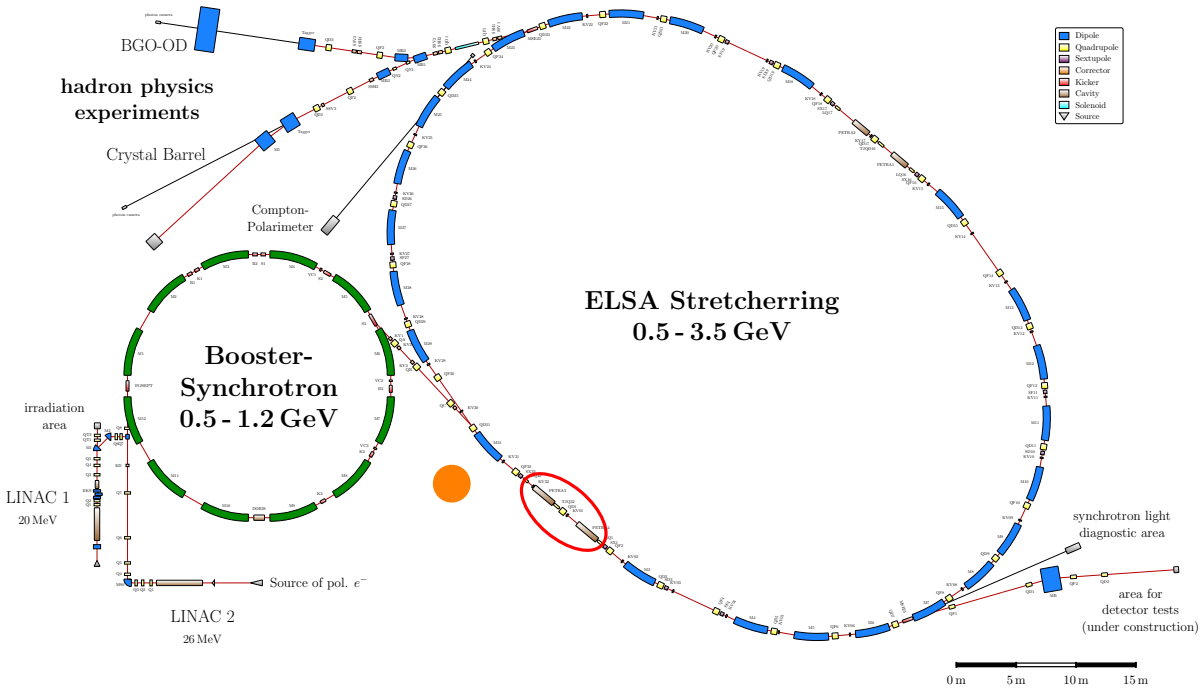

Figure 3.4 – Position of the new cavities in the stretcherring (red ellipse) and site of the new klystron (orange)

To get additional acceleration voltage two additional cavities will be incorporated in the strecher ring. The RF signals will be amplified by a additional klystron which will be controled by a digital low level radio frequency (LLRF) system. Waveguides will be used to transmit the power to the cavities. The next sections will give information about the used components and arrangements that where prepared. The location of the klystron and the position for the cavities in the accelerator tunnel can be seen in figure 3.4.

3.3.1 Cavities

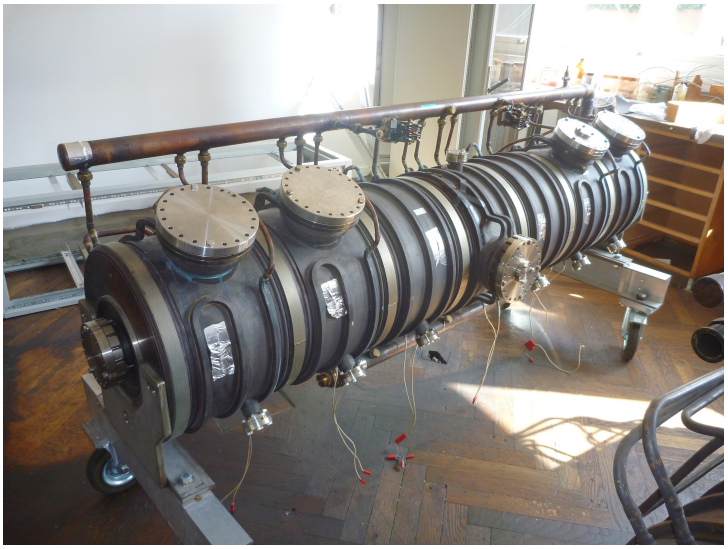

Figure 3.5 – Photograph of a PETRA seven cell cavity. [DES15]

As additional acceleration devices two seven cell PETRA type cavities will be used. The main parameters from the data sheet [DES15] are summed up in table 3.2 and a picture of a cavity is given in figure 3.5. Since their acceleration voltage is connected to the klystron power by the shuntimpedance

TM_{010} mode frequency @40 °C	499.67 MHz
Unloaded quality factor Q	32 800
Shunt impedance R_s	28.1 MΩ
Detuning due to temperature	8 kHz $°C^{-1}$
Nominal accelerating voltage	1.67 MV

Table 3.2 – Most important parameters of PETRA seven cell cavities as specified in the data sheet [DES15]

R_s a precise knowledege of this quantity is important. The cavities have been in storage for some years therefore impurities will have deposited on the inner surface. The quality factor and shunt impedance are than worsened, because the balancing currents of the fields flow only in the topmost layer of the copper in the cavity. If this layer is contaminated with dust or copper oxide the quality factor and shunt impedance lower. To get an information about these quantities they were measured by use of the bead pull method explained in the next chapter.

The only position in the strecherring where the cavities can be integrated is the straight section on the opposite side of the old RF-section (see figure 3.4). Two unused skew quadrupoles[1] have to be removed to get enough space for the cavities. For the separation of the two cavities the same constraint exists that their middle cells have to be separated by an integer multiple of the RF-wavelength like it is for the existing station. Only for this case the two acceleration voltages of the cavities can be summed together.

To tune the cavities to the proper resonance frequency two copper plungers [DESb] are used which can be driven in the RF-resonator by stepper motors. Since the plungers slightly change the geometry of the cavity the resonance frequency will change, too. They are mounted on the inner two of the flanges on

[1] Skew quadrupoles are special quadrupoles with their axis turned by forty-five degree

top of the cavity which are covered by blindflanges in figure 3.5. On the other two outside flanges two ion getter pumps have to be installed.

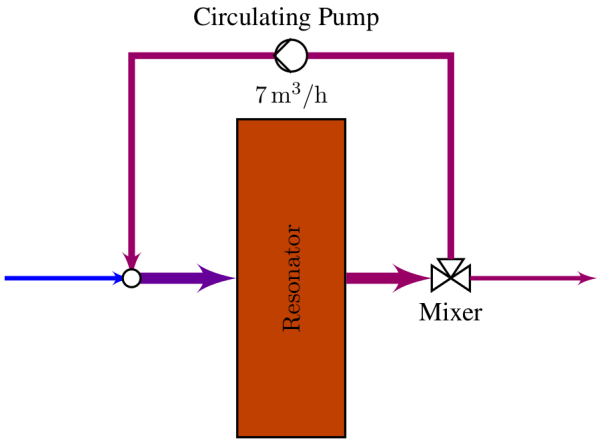

Figure 3.6 – Scheme of the cooling for the RF resonators [Sch15]

Cooling of the cavities is needed, since they heat up due to the balancing currents in their walls. The temperatures of the cavities have to be stabilized to one half of a degree celsius [Sau13]. Due to the change of the temperature the geometry of the cavities can change because of thermic expansion. The resonance frequency of the fundamental mode can be adjusted by movement of the plungers, but at some geometric circumstances higher order modes can be excited. Higher order modes are the modes with higher mode numbers *mnp* than the fundamental mode. These modes can build up fields in the cavities which can worsen the beam quality or result in total beam loss. Therefore they have to be watercooled to get out ouf this regions where dangerous higher order modes can build up. In the old RF-station a watercooling with variable bypass was integrated to ensure this. The new RF-station should be equipped with this bypass and circulating pump, too. To increase the temperature of the cavities the amount of water mixed in the circulating warm water, can be controlled by a mixing valve (Figure 3.6).

Bead pull measurements

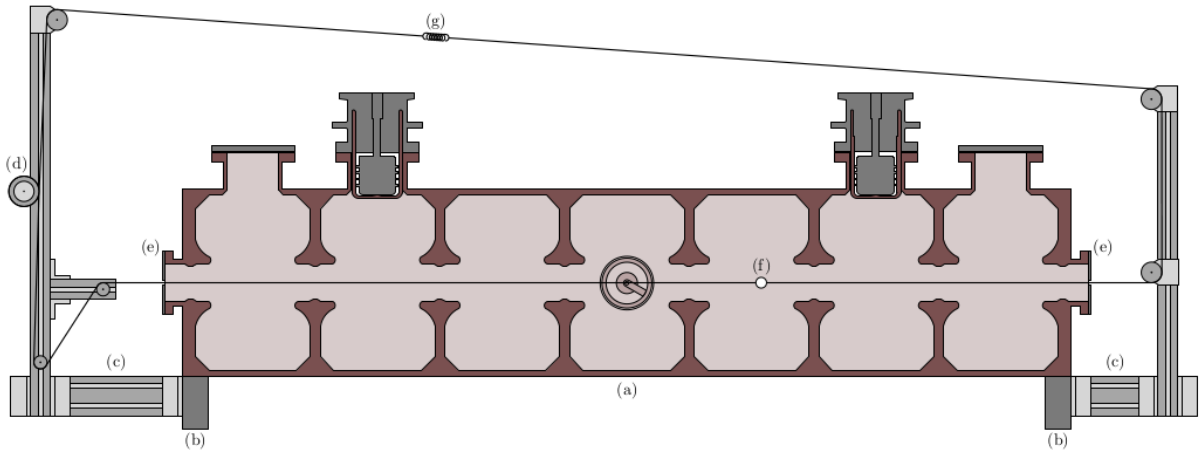

Figure 3.7 – Setup for a bead pull measurement of a PETRA seven cell cavity [Deu15]

The bead pull measurement is a specialized method to measure and derive the electric field inside a cavity. With this measurement technique the eletric field $E_0(z)$ in a cavity at the position z of the bead can be measured by the detuning $\Delta\omega(z)$ of the resonance frequency ω_0 of the cavity [Deu15]. This detuning arises because parts of the energy in the fields are transfered into the polarization of the bead.

$$E_0(z) = \sqrt{-\frac{4W_0}{\alpha_s} \cdot \frac{\Delta\omega(z)}{\omega_0}} \tag{3.7}$$

Where W_0 is the stored energy in the cavity and α_s is a constant only depending on the polarisation and geometric properties of the bead. The electric field for the acceleration mode was measured by moving the bead to different positions z in the cavity [Deu15]. When the electric field in the cavity is known, the acceleration voltage U' for a particle can be calculated as the integral over the length of the cavity (equation 2.8).

$$U' = \int_0^L E_0(z)\,\mathrm{d}z \tag{3.8}$$

While the electrons pass through the cavity the alternating electric field first builds up and than reduces. Since the electrons are only accelerated by the present field the effective acceleration voltage lowers. To get the effective acceleration voltage U_{cav} which describes the voltage that the electrons are really exposed, the voltage U' has to be weighted with the transition time factor Λ (Equation 2.10) .

$$U_{cav} = \Lambda \cdot U' \tag{3.9}$$

Since the energy gain of the electrons $\Delta E = q \cdot U_{cav}$ is only induced by the effective voltage U_{cav} the shunt impedances of the cavities are also indicated as effective shunt impedance R_s.

$$R_s = \frac{U_{cav}^2}{2 \cdot P} = \frac{(\Lambda U')^2}{2 \cdot P} = \Lambda^2 \cdot R_s' \tag{3.10}$$

The measured effective shunt impedances are $(25.65 \pm 0.59)\,\mathrm{M\Omega}$ for the PETRA-III cavity and $(24.47 \pm 0.87)\,\mathrm{M\Omega}$ for the PETRA-IV cavity, which will be used in the new RF station (measured in [Deu15]). The average effective shunt impedance is:

$$R_s = (25.06 \pm 0.59)\,\mathrm{M\Omega} \tag{3.11}$$

3.3.2 Coupling

The coupling from the RF power into the cavity is performed by a coupling loop. To change this factor the coupling loop (Figure 3.8) has to be rotated which means the vacuum system of the cavities has to be broken. So the coupling factor has to be adjusted before the cavities are installed in the stretcher ring. The calculation of the required coupling factors will be performed in chapter 4.6.

3.3.3 Doorknob-coupler

The doorknob coupler is a component of the system which matches the transition from the koaxial coulping loop to the rectangular waveguide. One doorknob coupler [DESa] for the coupling loops [DES11] which fit to the PETRA seven cell cavities exists but two are needed. Other types of doorknob couplers with fitting coupling loops (figure 3.9) are available. If the required coupling factors can be reached

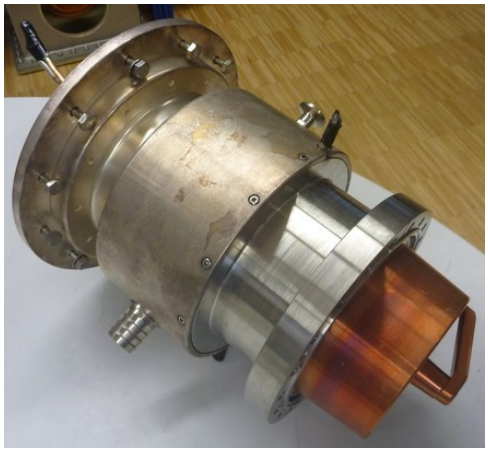

Figure 3.8 – Photoraph of a coupling loop for PETRA type cavities

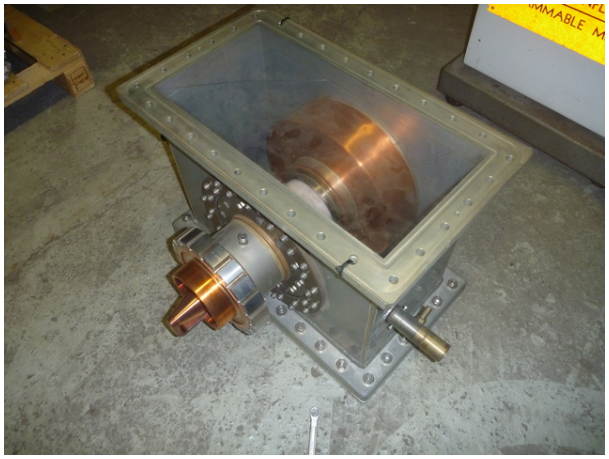

Figure 3.9 – So called CERN-Coupler with fitting coupling loop.

with this loops has to be shown but first a adapter from the coaxial line of the loop to a standart of measurement cables has to be produced.

3.3.4 Waveguides

To transmit the RF power from the generator to the cavities WR1800 waveguides will be used. The cutoff frequency of waveguides can be written as follows (Section 2.4).

$$f_c = \sqrt{\left(\frac{mc}{2a}\right)^2 + \left(\frac{nc}{2b}\right)^2} \tag{3.12}$$

Waves with lower frequencies than this frequency cannot propagate through the waveguide. WR1800 waveguide have an inner width of 18″ and a height of 9″ [DES05], what corresponds to 45.72 cm and 22.86 cm. The cutoff frequency of the fundamental TE_{10} mode therefore is $f_c^{TM_{10}} = c/2a \approx 328\,\text{MHz}$. Therefore transmission of 500 MHz RF-power through WR1800 waveguides is possible (see for example figure 2.7). The transmission of the RF-power has been simulated for different cornered and bend waveguides to show that they do not reflect any power (for example seen in figure 3.10). It turns out, that

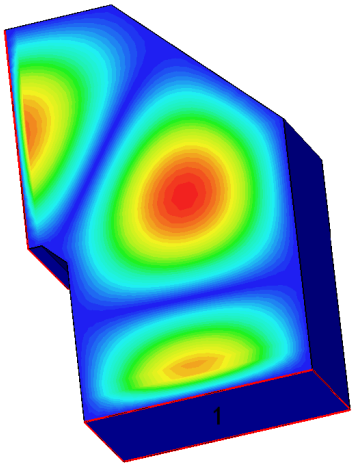

Figure 3.10 – Absolute fieldstrength of the electric field in a cornered waveguide simulated with *CST Microwave studio*. High field strength are depicted in red lower in blue.

the damping of every bend and straight waveguide is less than −30 dB which means less than 1 ‰.

All the available waveguides have been cataloged to plan the waveguide transition from the klystron to the cavities. The ELSA tunnel has been surveyed with all the components which cannot be removed. From this a model of the tunnel was developed. The planed setup can be found in figure 3.11 and with the model of the tunnel in figure 3.12. The height of the ceiling leaded to no straight waveguide connection between the two incouplings of the cavities. The two arms of the waveguides had to be bend down, so that the feed line fits under the ceiling.

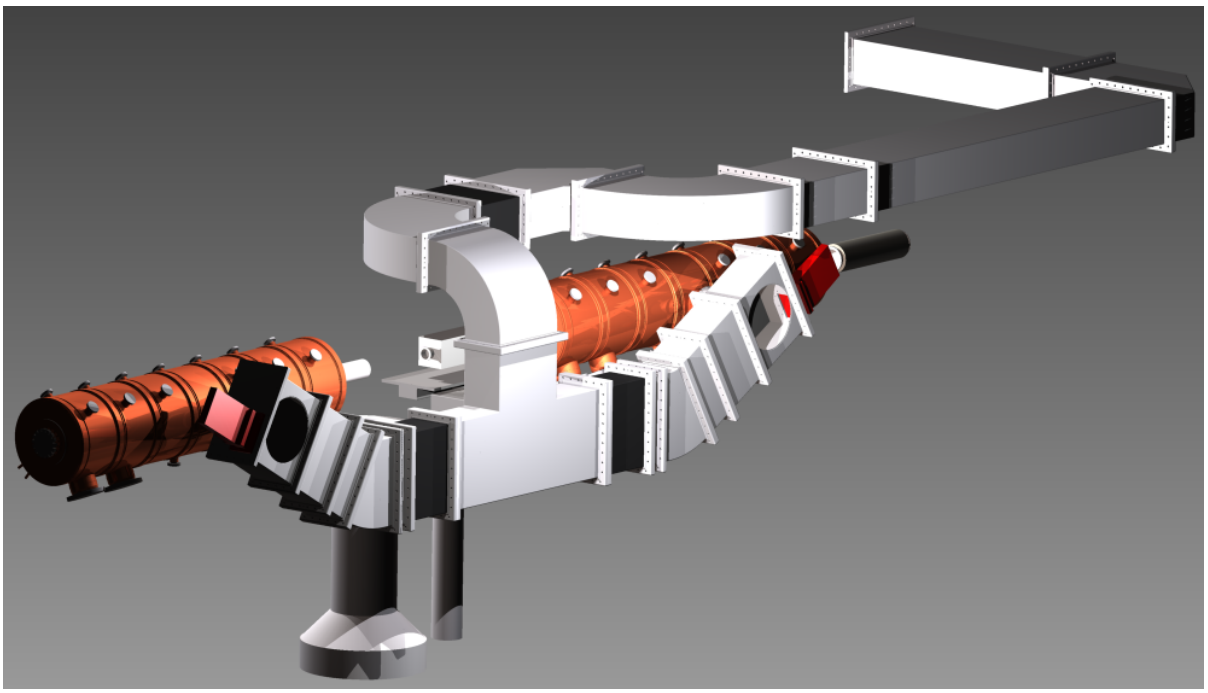

Figure 3.11 – Planed setup for the waveguide transition of the new RF-station. (P. Hänisch)

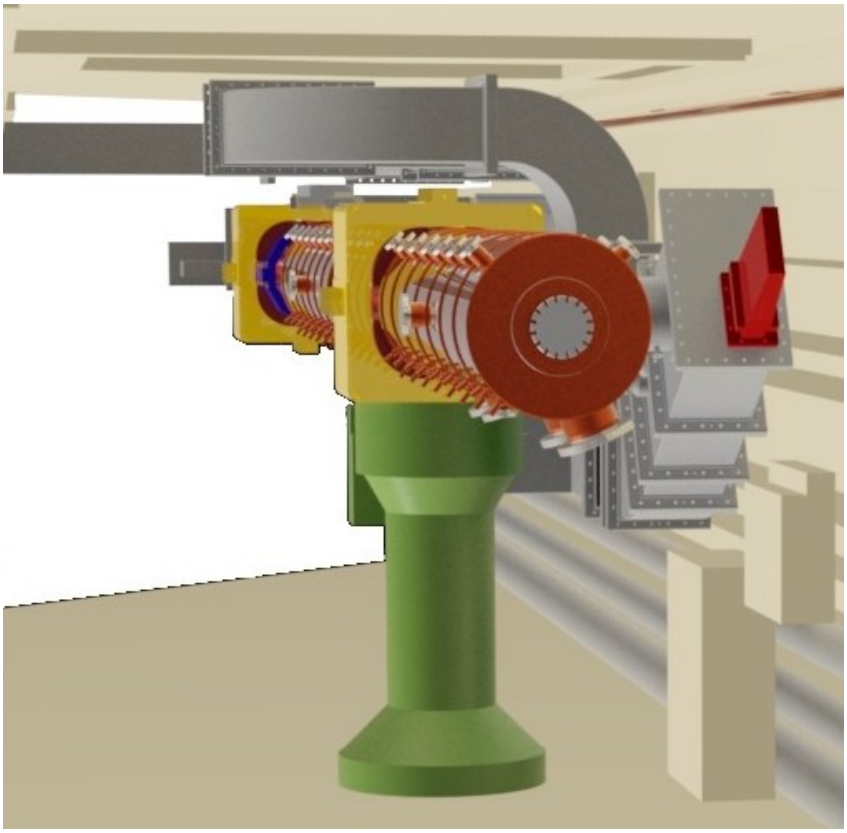

Figure 3.12 – Components of the second RF-station in the ELSA tunnel. (P. Hänisch)

3.3.5 Klystron

To generate the high power RF signal for the additional station, a Thomson-CSF F2055 Klystron [Tho81] which is the same klystron type like the one of the existing station, will be used. The high voltage power supply for the electron gun of the klystron has already been build up and can be seen in figure 3.13. To prevent damage of the klystron a circulator (Figure 3.14) will be build in between the klystron and the magic T to build a waveguide diode.

3.3.6 Low level radio frequency signal generation

To control the phase and the amplitude in the cavities a digital LLRF-system is used. The system is the LLRF9/500 manufactured by Dimtel, Inc [Tey]. Nine analog input signals such as forward and backward power in the waveguides and field strength in different cells of the cavities are digitalized to capture the actual state of the RF-station. The digitalized signals are processed to drive the klystron and control the plungers. By an internal phase delay the required phase between the new and the existing RF-station can be adjusted.

Another possibility provided by the LLRF system is to set thresholds for the reflected powers in the waveguide system. If one of these thresholds is exceeded the LLRF system will switch off the klystron to prevent damage of components of the whole acceleration station.

Figure 3.13 – Klystron site with high voltage power supply on the left site and klystron on the right. The rectangular incoupling in the WR1800 waveguide can be seen on the right site of the klystron.

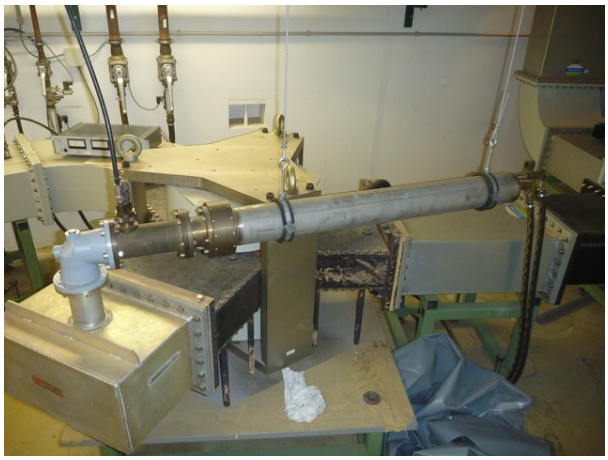

Figure 3.14 – Cirulator for WR1800 waveguides. The Forward power comes from the left and is transmitted to the right. Reflected power from the right is damped in the watercooled load in the front.

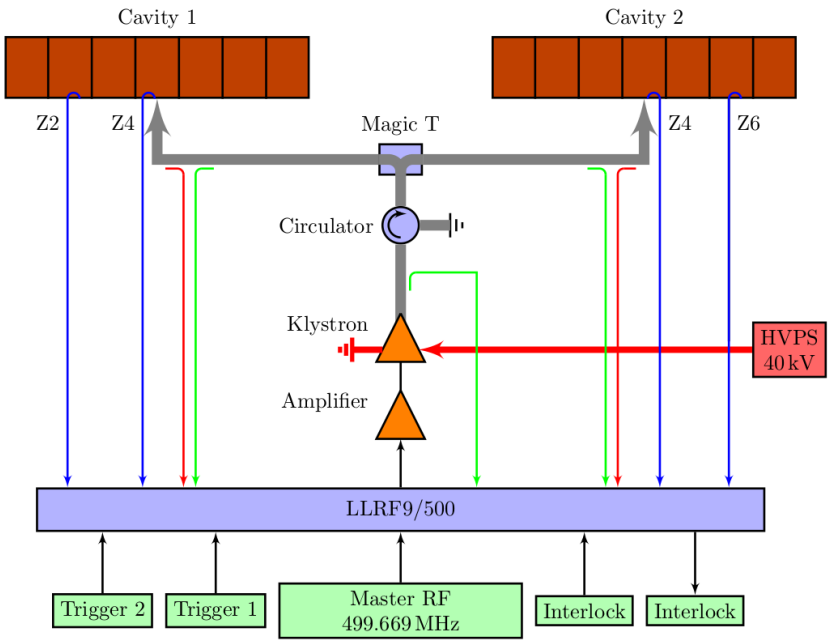

Figure 3.15 – Schematic setup of the LLRF-system which will be used ad the second RF-station. [Sch+15b]

CHAPTER 4

Operational interaction of two RF stations

4.1 Second radio frequency station

To increase the available power two additional seven cell cavities will be installed into the stretcherring. In the old station and future second station different cavities with different shunt impedances will be used. Hence one has to think about how to distribute the acceleration voltage and how to choose the phase relation between the different stations. Therefore we at first have to think about the motion of the particles in the compound RF-potential.

The total acceleration voltage U_{tot} for the particles can be described as the sum of the voltages of two RF stations U_1 and U_2.

$$U_{\mathrm{tot}}(\phi) = U_1(\phi) + U_2(\phi + \Delta\phi_{\mathrm{RF}}) \tag{4.1}$$

$$= 2U_{1,\mathrm{cav}} \sin(\phi) + 2U_{2,\mathrm{cav}} \sin(\phi + \Delta\phi_{\mathrm{RF}}) \tag{4.2}$$

Since in both stations the cavities will be separated by an integer multiple of the RF wavelength the total peak acceleration voltage of one station can be described as $U_i = 2 \cdot U_{i,\mathrm{cav}}$. The phase difference between the two RF stations is an additional degree of freedom. If $\Delta\phi_{\mathrm{RF}} = 0$ the two rf stations oscillate in phase and their voltages can be summed together. For the other extreme $\Delta\phi_{\mathrm{RF}} = \pi$ the voltages would exactly cancel and the total acceleration voltage would be equal to zero.

4.1.1 Longitudinal beam dynamics with two RF-stations

For the longitudinal oscillation of the particles in the bucket the same equation of motion can be derived as in the RF potential of one station (see appendix A.2.3 for derivation and equation 2.32 for comparison).

$$\frac{\mathrm{d}^2\Delta\phi}{\mathrm{d}t^2} + 2\alpha_s \frac{\mathrm{d}\Delta\phi}{\mathrm{d}t} + \Omega_s^2 \Delta\phi = 0 \tag{4.3}$$

The equation of motion is exactly the same, but the synchrotron frequency f_s differs from the frequency in case of one RF station (Equation 2.33).

$$f_s = \frac{\Omega_s}{2\pi} = \sqrt{\frac{h\eta e}{\pi\beta^2 T_0^2 E_0}\Big(U_{1,\mathrm{Cav}} \cos(\phi_0) + U_{2,\mathrm{Cav}} \cos(\phi_0 + \Delta\phi_{\mathrm{RF}})\Big)} \tag{4.4}$$

Also in the potential an additional term occurs compared to equation 2.34.

$$V(\Delta\phi) = \frac{-2e\beta^2 E_0}{\pi h\eta}\Big(U_{1,\mathrm{cav}}\big(\cos(\phi+\Delta\phi)+\Delta\phi\sin(\phi)\big)+U_{2,\mathrm{cav}}\big(\cos(\phi+\Delta\phi_{\mathrm{RF}}+\Delta\phi)+\Delta\phi\sin(\phi+\Delta\phi_{\mathrm{RF}})\big)\Big) \tag{4.5}$$

The overvoltage factor q can also be written for two combinated RF stations (compare equation 2.35):

$$q = \frac{2U_{1,\mathrm{cav}}+2U_{2,\mathrm{cav}}}{2U_{1,\mathrm{cav}}\sin(\phi_0)+2U_{2,\mathrm{cav}}\sin(\phi_0+\Delta\phi_{\mathrm{RF}})} \tag{4.6}$$

In the calculations for the operation of the two stations the synchrotron frequency f_s will be the used parameter instead of q since they both describe the beam lifetime similarly.

4.2 Software for cavity field parameters

Since the used cavities differ by their shuntimpedance $R_{\mathrm{s},1}$ and $R_{\mathrm{s},2}$, it is not the most efficient way to run the accelerator dividing the acceleration voltage in two equal parts. To investigate the power consumption and therefore get the best efficiency one introduces a variable ϵ_2:

$$\epsilon_2 = \frac{2U_{2,\mathrm{cav}}}{2U_{1,\mathrm{cav}}+2U_{2,\mathrm{cav}}} = \frac{U_{2,\mathrm{cav}}}{U_{1,\mathrm{cav}}+U_{2,\mathrm{cav}}} \tag{4.7}$$

This factor describes which portion of the maximal acceleration voltage the new second RF-station takes. For $\epsilon_2 = 0$ the case without a second station is described. $\epsilon_2 = 1$ means that the old RF-station is turned off and the accelerator runs only with the acceleration of the new station. The voltage in the second station can be described in terms of ϵ_2 and the voltage in the first RF-station.

$$U_{2,\mathrm{cav}} = \left(\frac{\epsilon_2}{1-\epsilon_2}\right)U_{1,\mathrm{cav}} \tag{4.8}$$

With this factor the total acceleration voltage U_{tot} (equation 4.2) can be written as follows:

$$U_{\mathrm{tot}}(\phi) = 2U_{1,\mathrm{cav}}\sin(\phi)+2\left(\frac{\epsilon_2}{1-\epsilon_2}\right)U_{1,\mathrm{cav}}\sin(\phi+\Delta\phi_{\mathrm{RF}}) \tag{4.9}$$

$$= 2U_{1,\mathrm{cav}}\left(\sin(\phi)+\left(\frac{\epsilon_2}{1-\epsilon_2}\right)\sin(\phi+\Delta\phi_{\mathrm{RF}})\right) \tag{4.10}$$

The overall used RF power is the sum of the powers of both stations:

$$P_{\mathrm{tot}} = P_1 + P_2 \tag{4.11}$$

$$= P_{1,\mathrm{beam}} + P_{1,\mathrm{field}} + P_{2,\mathrm{beam}} + P_{2,\mathrm{field}} \tag{4.12}$$

$$= 2U_{1,\mathrm{cav}}\sin(\phi_0)\cdot I_{\mathrm{beam}} + 2\frac{U_{1,\mathrm{cav}}^2}{2R_{\mathrm{s},1}} + 2U_{2,\mathrm{cav}}\sin(\phi_0+\Delta\phi_{\mathrm{RF}})\cdot I_{\mathrm{beam}} + 2\frac{U_{2,\mathrm{cav}}^2}{2R_{\mathrm{s},2}} \tag{4.13}$$

The reference phase ϕ_0 and the voltages needed at the two stations can be fixed by two conditions for the synchrotron frequency f_s and revolution voltage U_{rev}:

$$f_s = \frac{\Omega_s}{2\pi} = \sqrt{\frac{h\eta e U_{1,cav}}{\pi\beta^2 T_0^2 E_0}\left(\cos(\phi_0) + \left(\frac{\epsilon_2}{1-\epsilon_2}\right)\cos(\phi_0 + \Delta\phi_{RF})\right)} \tag{4.14}$$

$$U_{rev} = 2U_{1,cav}\left(\sin(\phi_0) + \left(\frac{\epsilon_2}{1-\epsilon_2}\right)\sin(\phi_0 + \Delta\phi_{RF})\right) = \frac{e\beta^3}{3\varepsilon_0 (m_o c^2)^4}\frac{E_0^4}{R} \tag{4.15}$$

To solve the system of equations 4.14 and 4.15 a program was written (Figure 4.1). It solves the system of equations for ϕ_0 and $U_{1,cav}$. The software was written in Python and was given the name `hfplotter`[1]

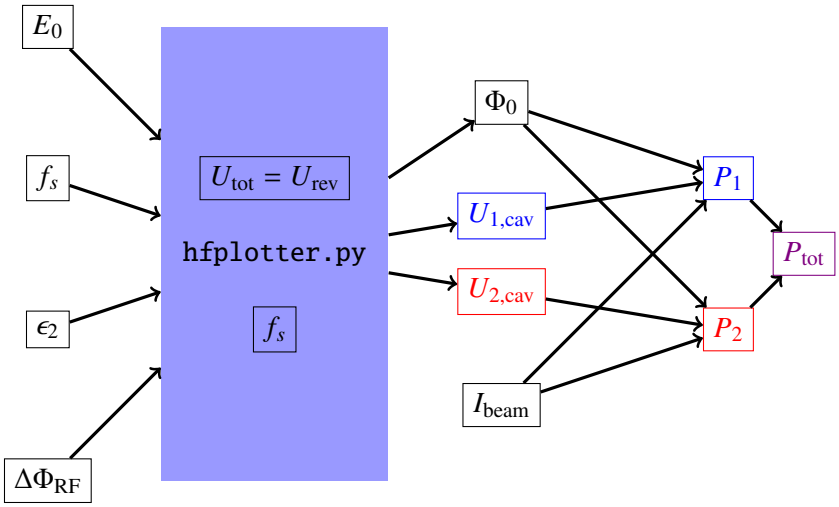

Figure 4.1 – Input and output data of the software `hfplotter.py` and processing of these data

because it at first only plotted RF voltages for different phases. The input and output parameters of the software are given in table 4.1. Now to derive the needed voltages in the cavities $U_{1,cav}$, $U_{2,cav}$ and

Input	Output
E_0	ϕ_0
f_s'	$U_{1,cav}$
ϵ_2	$U_{2,cav}$
$\Delta\Phi_{RF}$	P_1
I_{beam}	P_2
	P_{tot}

Table 4.1 – Input and output parameters of the software `hfplotter`

the reference phase ϕ_0 it at first calculates the revolution voltage U_{rev} from the given beam energy E_0. The system of equations of 4.14 and 4.15 can be solved mathematically for $U_{1,cav}$ and ϕ_0. But since many inverse trigonometrical functions have to be used mathematically solutions with many signs exist. Therefore `hfplotter` checks which combination of signs solves the conditions 4.14 and 4.15. After that with given ϵ_2, $U_{2,cav}$ is calculated with equation 4.8 and solitions for the voltages and phases in both stations have been found (see for example figure 4.2) . An interface was developed where the parameters

[1] HF is a german shortcut equivalent to the english RF.

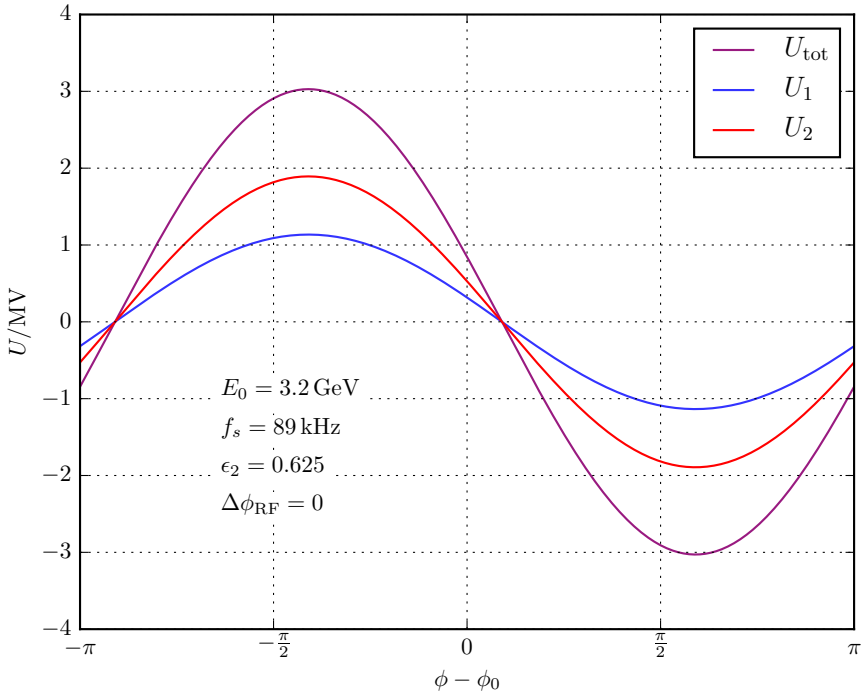

Figure 4.2 – Voltages of the two RF-Stations for typical parameters and no phase difference between the two stations

E_0, $\Delta\phi_{\mathrm{RF}}$, ϵ_2 and f_s can be adjusted and the resulting voltages and the RF-potential can be observed (figure 4.3). From the needed voltages with additional knowledge of the beam current I_{beam} the needed power can be calculated.

In plots which show the needed powers there are regions marked in deep red to show that an operation with these parameters would not work. There are two reasons why some areas have to be excluded from the working parameters: At first regions have been canceled where the klystron output power of at least one klystron ought to be higher than 200 kW. Powers higher than 200 kW are unable to be produced by the used klystrons (Section 3.3.5). Additionally areas have been canceled where the accelerating voltage on reference phase is below zero: If the particles pass the cavities on a phase where the accelerating voltage is negative $U_i \sin(\phi_0) < 0$ the particles would be decelerated what leads to a negative beam loading $P_{\mathrm{beam}} = U_i \sin(\phi_0) \cdot I_{\mathrm{beam}} < 0$. Since the cavity in this considerations is coupled to the transmission line perfectly this power would be transmitted in the waveguide system. To protect the klystron from damage by dint of reflected power in the waveguide system the LLRF-system would switch of the klystron. Even if the LLRF-system would not switch of the klystron the outcoupled power would be damped in the termination at the circulator, which saves the klystron from damage.

4.3 Operation without phase difference

4.3.1 Efficiency

In figure 4.4 the RF-power which the klystrons have to generate is ploted with respect to the voltage divider factor ϵ_2. A beam current of 40 mA and the energy of 3.2 GeV were chosen. It can be seen that for $\epsilon_2 = 0$ the needed power is barely under 200 kW which is the limitation due to the maximum klystron output power. This is why the beam current and energy where chosen in this way. For this parameters the acceleration in ELSA works just with the existing RF station. So the power requirements for acceleration

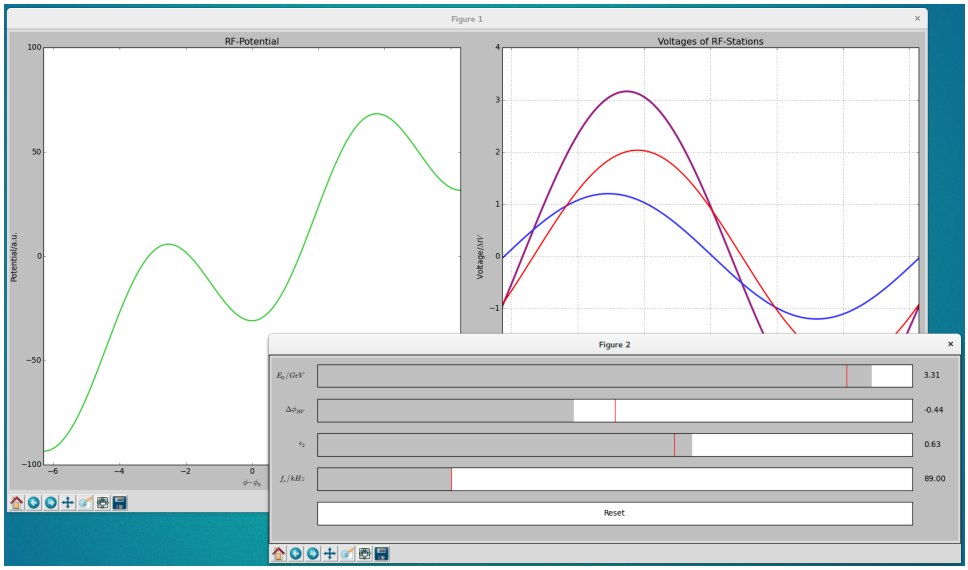

Figure 4.3 – Graphical user interface for the calculation of the voltages in both stations. In the left plot the RF-Potential and in the right the voltages of both stations (red,blue) and the resulting total voltage (purple) can be seen. The main input parameters for the calculation can be adjusted by the sliders.

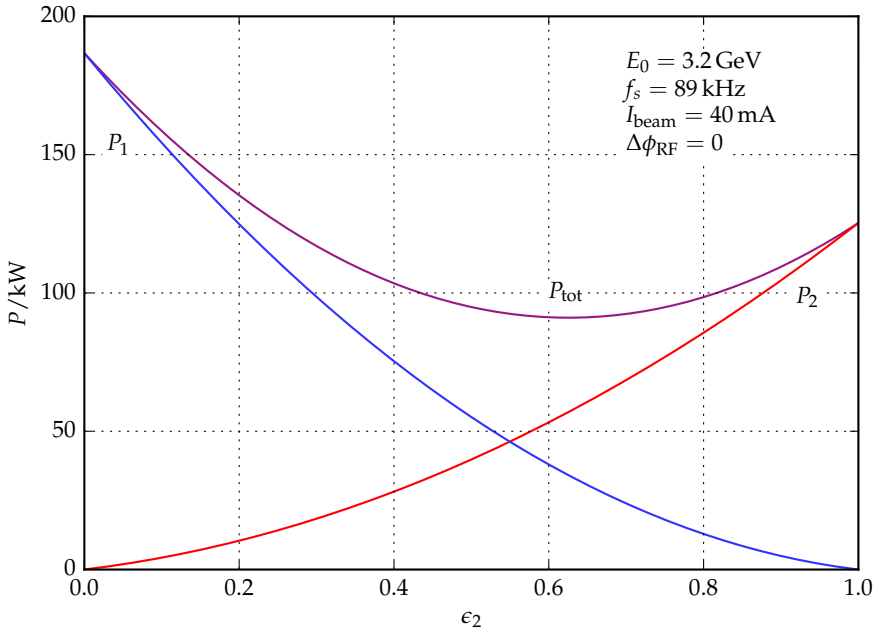

Figure 4.4 – Powers P_1 and P_2 which the two klystrons of the stations have to generate to accelerate a 40 mA beam current at an energy of 3.2 GeV with $\Delta\phi_{\mathrm{RF}} = 0$. P_{tot} is the sum of the powers of both stations.

with one station can be compared with the operation with two RF stations. As expected the minimal needed power is not at the point where the voltage is splitted in two equal halves at $\epsilon_2 = 0.5$ as expected but at $\epsilon_2^{\text{opt}} = 0.625$. This is due to the differences in the shuntimpedances of the used cavities. If the accelerator would be driven with a beam current of 40 mA at an energy of 3.2 GeV with the two stations at the the optimum voltage distribution ϵ_2^{opt} one saves more than half of the RF power with respect to the operation with the old station only. In beam times were not so high beam currents are required a hugh amount of RF power and therefore electricity expenses can be saved. The optimum operation parameters to get the best efficiency which is the minimum in figure 4.4 can be seen in table 4.2.

$\Delta\phi_{\text{RF}}^{\text{opt}}$	0
ϵ_2^{opt}	0.625

Table 4.2 – Optimum operation parameters for two RF stations

4.3.2 Beam current

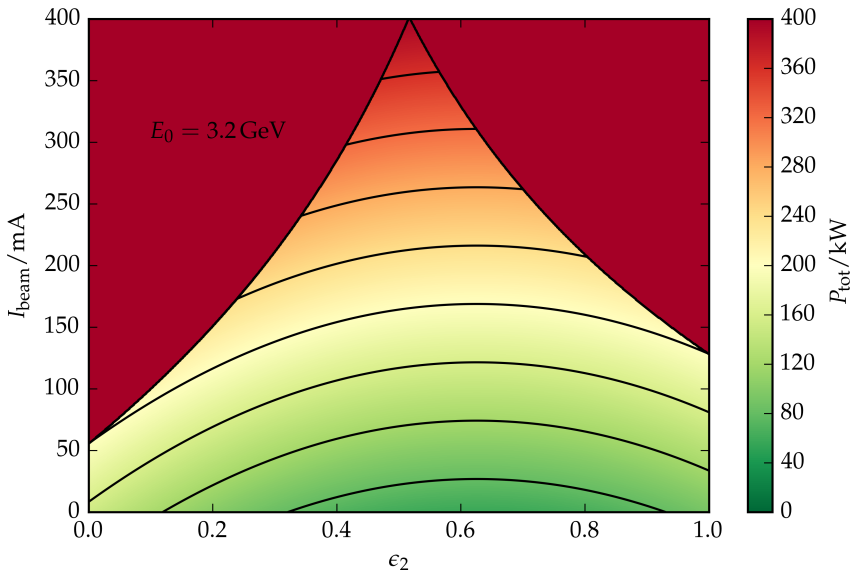

Figure 4.5 – Storable beam current in ELSA at an energy of 3.2 GeV with no phase difference between the two RF-stations. Technically not operatable regions are marked in deep red.

The storable beam current depends on the provided RF-power (Equation 4.13). The extension of the available RF-power will be done to enhance the internal beam current in ELSA at an energy of 3.2 GeV to 200 mA. In figure 4.5 the needed RF power for different ϵ_2 and beam currents at 3.2 GeV can be seen. Technically not operable regions are marked in deep red. For the most efficient ϵ_2 it will be no problem to store a beam current of 200 mA. The total needed RF power will be approximately 240 kW, it can be read off in figure 4.5. Additionally a plot of the possible operational region at 3.2 GeV with 200 mA of beam current can be found in the appendix in figure A.4.

4.3.3 Synchrotron frequency

The synchrotron frequency f_s of 89 kHz was fixed up to this point. If there is more power available one could think about enhancing the synchrotron frequency to increase the quantum lifetime of the beam

(section 2.6.4). The needed power depending on the synchrotron frequency f_s and the beam energy E_0 for a beam current of 200 mA can be seen in figure 4.6. It shows that the synchrotron frequency of an

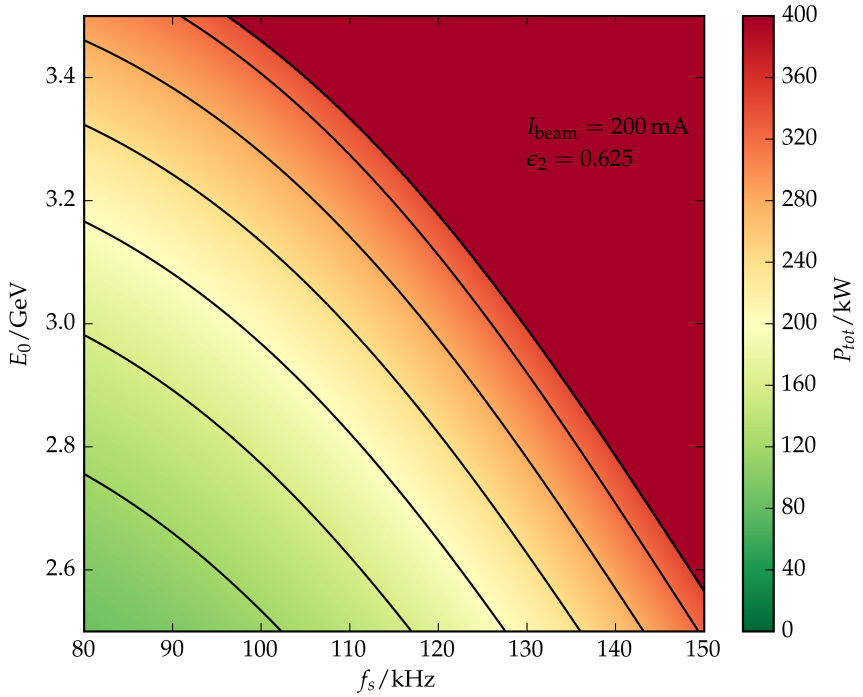

Figure 4.6 – Klystron power for a beam current of 200 mA depending on the synchrotron frequency f_s and the beam energy E_0. Technically not operatable regions are marked in deep red.

stored beam current of 200 mA at 3.2 GeV could be raised to 115 kHz but comes with a raise auf the needed power from under 240 kW to 320 kW. The beam lifetime χ_s dependent on beam energy E_0 and synchrotron frequency f_s can be seen in figure 4.7. Since the beam lifetime at 3.2 GeV and synchrotron

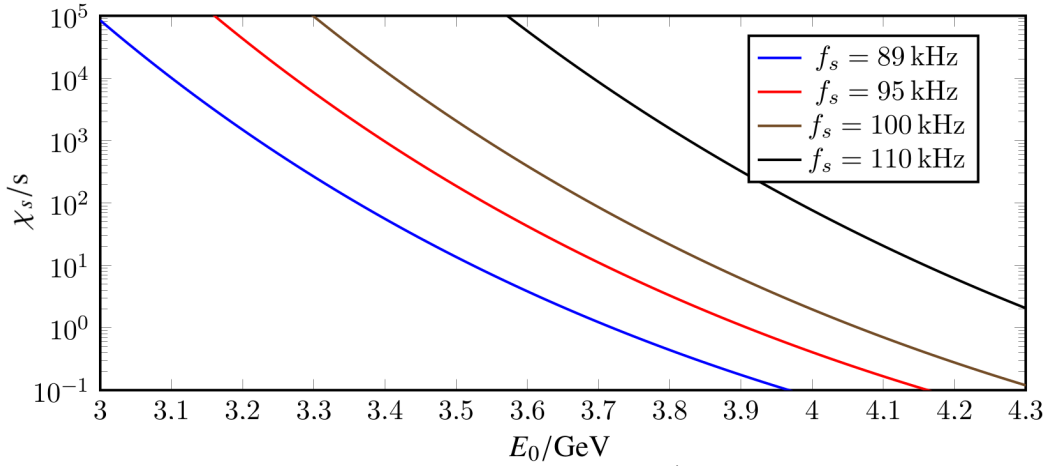

Figure 4.7 – Beam lifetime χ_s of beams with different synchrotron frequencies f_s depending on their energy E_0 [Sch15]

frequency of 89 kHz is already above 10^3 s (Figure 4.7) which is approximately 16 minutes, it is not necessary to raise the synchrotron frequency in the booster mode, where the electrons are stored for only

up to one minute. Only for the storage mode, where lifetimes of up to hours are wanted, an increasment of the synchrotron frequency is reasonable.

4.4 Phase stability at injection energy

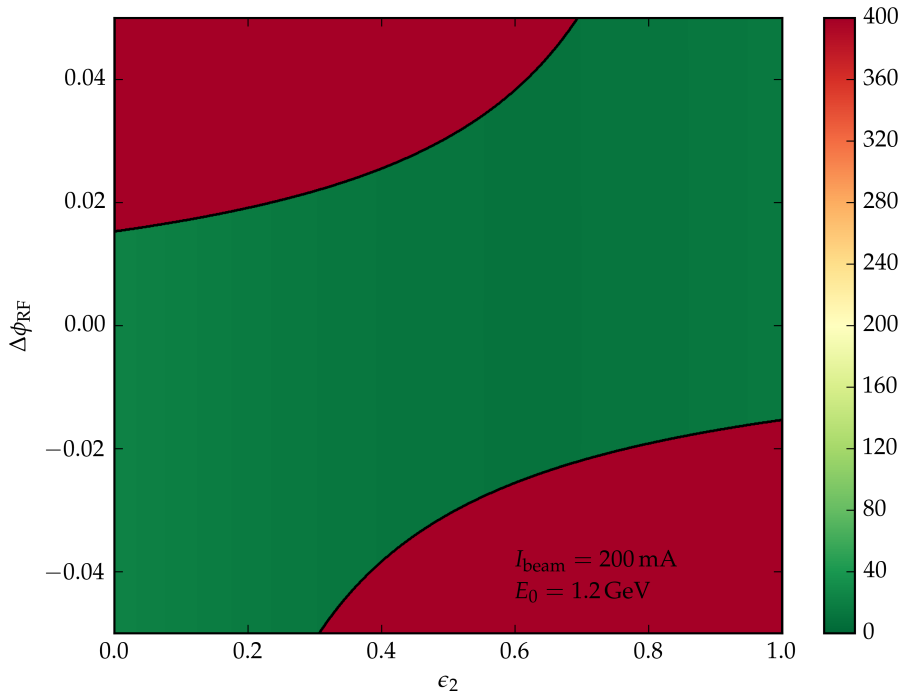

Figure 4.8 – Acceptable parameters at injection energy

The possible operation parameters for a beam current of 200 mA at 1.2 GeV can be found in figure 4.8. It has to be mentioned that the axis with the phase difference between the stations is zoomed in. The unzoomed version of this plot can be found in the appendix A.3. Figure 4.8 shows that the discrapancy from the optimum phase $\Delta\phi_{RF} = 0$ at $\epsilon_2 = 0.625$ should not be bigger than 0.04 and not be smaller than -0.02. The narrow region is because of the very small reference phase at injection energy. A small reference face leads fastly to a negative acceleration voltage what gives rise for reflections. The maximum difference of 0.02 leads to a needed phase stability of the second RF station of under 1.1° if one wants to avoid reflections from the cavities.

4.5 Operation with phase difference

The phase difference between the two stations can be chosen by an internal phase shifter in the LLRF (chapter 3.3.6). One can figure out operational modes where the two RF stations are running with different phases, one example is given in figure 4.9. With a phaseshift of $\Delta\phi_{RF} = -0.45$ between the stations the beam loading P_{beam} in station one becomes zero. In this case power is only needed to build up the electric field in the cavities, what leads to a higher overvoltage factor and therefore beam lifetime. The station with no beam loading can be seen as a type of focusing cavity which does not compensate any losses of the electrons but only keeps them together as a bunch. The needed total power with respect to this phase $\Delta\phi_{RF}$ and to ϵ_2 can be seen in figure 4.10. Technically not operable regions are markes in

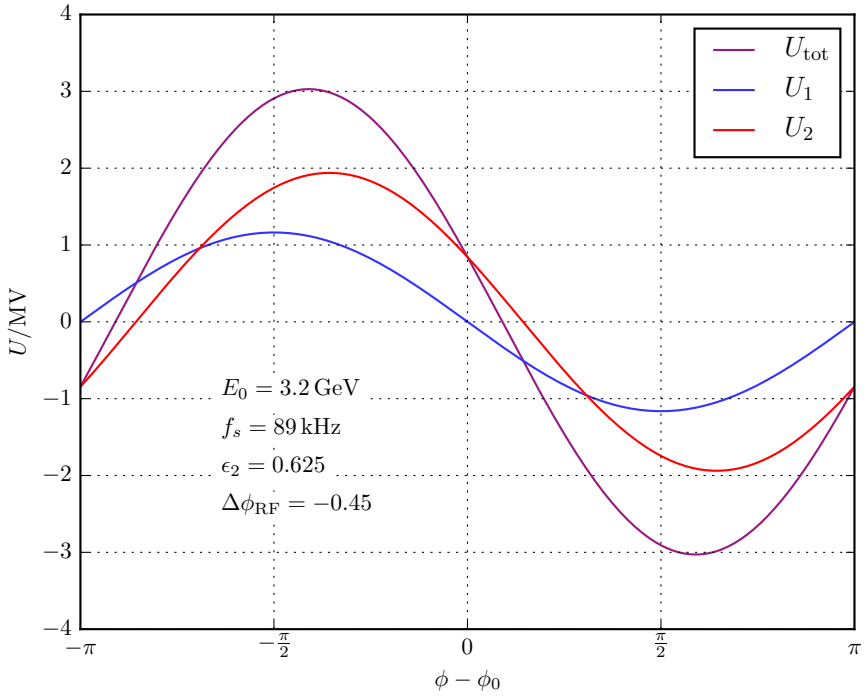

Figure 4.9 – Accelerating voltages with phase difference chosen in a way that in station one the beam loading vanishes. This means the acceleration voltage on the reference phase is zero in station one

deep red as explained in section 4.2. To understand why some regions have to be excluded in figure 4.11 the needed powers to build up the field in station one $P_{1,\mathrm{field}}$ and the power due to beamloading $P_{1,\mathrm{beam}}$ can be seen separately. The needed power of the first klystron has a kink at $\epsilon_2 = 0.625$ where the needed power due to beam loading becomes negative. Since the needed acceleration voltage for bigger ϵ_2 would be negative (can be seen in figure 4.12). This would lead to reflected power in the waveguide system and lead to a shutdown of the klystron by the LLRF system. Therefore negative powers do not have to be subtracted from the needed klystron power but in this case are set to zero and kinks in the needed power arise. The region in figure 4.10 which is not depicted in deep red is the region with the possible operation parameters to store a beam current of 40 mA at an energy of 3.2 GeV. Since the most efficient phase difference is zero $\Delta\phi_{\mathrm{RF}} = 0$ the following considerations will be done for this phase.

4.6 Coupling factor

All these calculations have been performed for a reflectionless coupling between the cavities and waveguides. The optimum coupling factor is dependend on the power of the beam and the field as explained in chapter 2.3.1. For the optimum coupling factor one gets (see equation 2.18):

$$\kappa_{\mathrm{opt}} = 1 + \frac{P_{\mathrm{beam}}}{P_{\mathrm{field}}} \tag{4.16}$$

But the fraction $P_{\mathrm{beam}}/P_{\mathrm{field}}$ for the optimum voltage divider factor $\epsilon_2^{\mathrm{opt}}$ depends on the beam current and the energy as it can be seen in table 4.3.

The software could be used as a basis for further calculations in which the influence of the coulping factor on the reflected powers is considered, to get more information about operational modes with phase

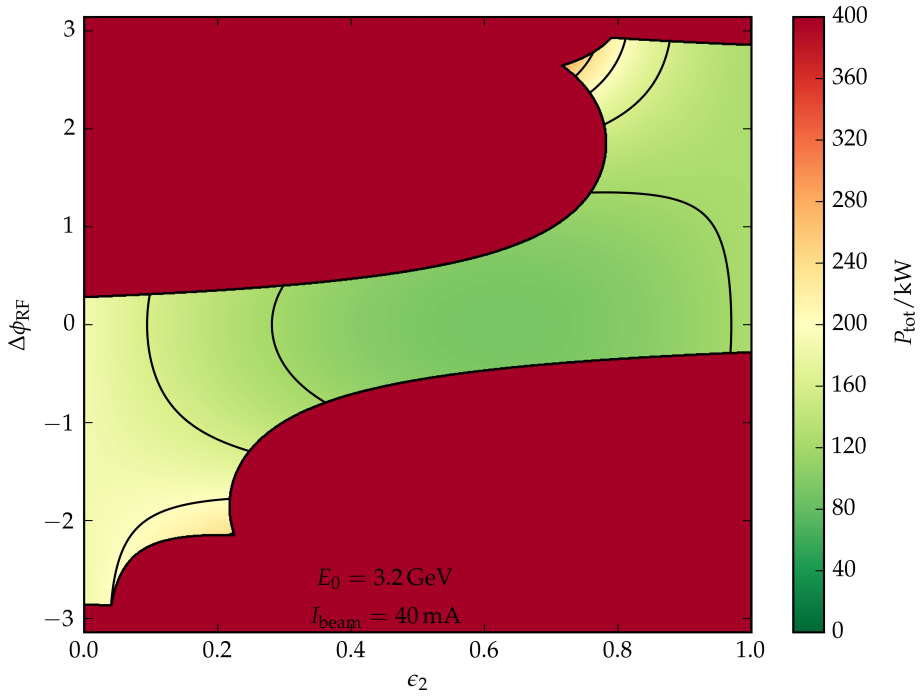

Figure 4.10 – Total klystron power needed to accelerate a 40 mA beam at 3.2 GeV. Plots without these exclusions can be found in the appendix.

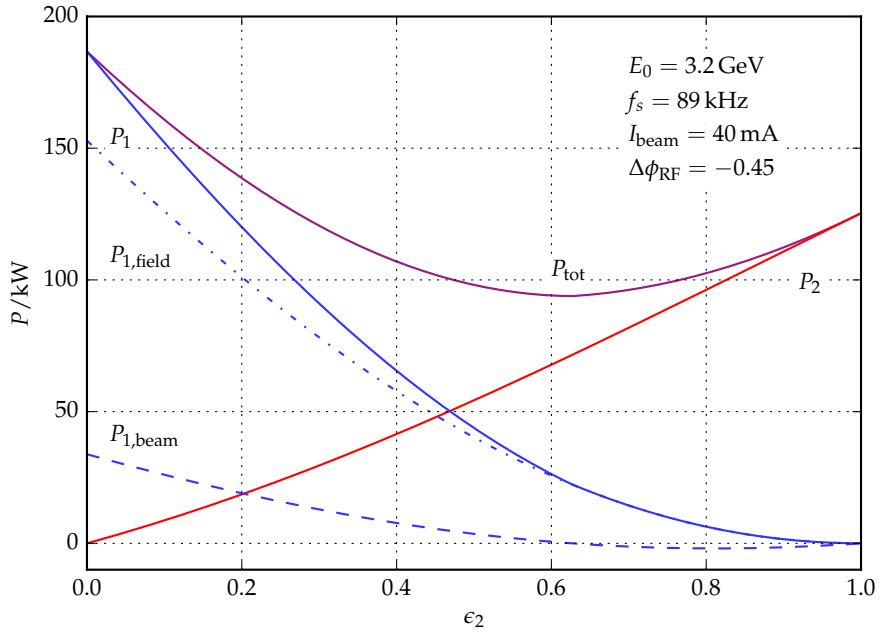

Figure 4.11 – Needed power of the klystrons with a phase difference of both stations of $\Delta\phi_{\mathrm{RF}} = -0.45$.

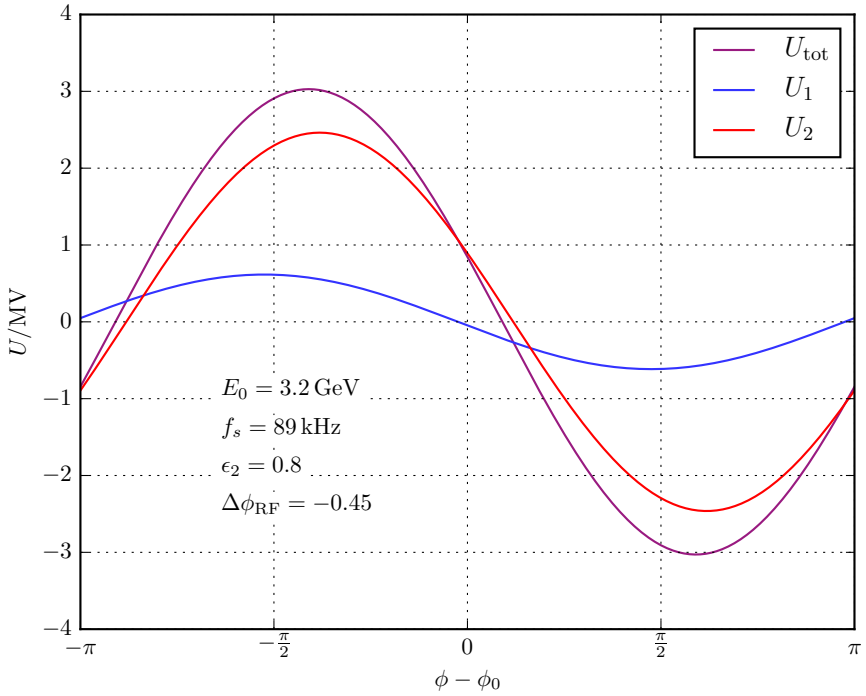

Figure 4.12 – Negative reference voltage in one RF-station.

E_0/GeV	I_{beam}/mA	$P_{\mathrm{beam}}/P_{\mathrm{field}}$	κ_{opt}
3.2	200	2.95	3.95
1.2	200	0.45	1.45
3.2	20	0.33	1.33
1.2	20	0.05	1.05

Table 4.3 – Optimum coupling factors for different beam currents and energies for the new cavities at $\epsilon_2^{\mathrm{opt}}$

differences between the RF stations.

To sum up the reflections about the operation parameters one can say that it will be possible to store a beam of 200 mA at an energy of 3.2 GeV. Therefore it will be possible to enhance the event rate at the experiments by one order of magnitude. The most efficient adjustment would be with no phase difference between the two RF-stations $\Delta\phi_{\mathrm{RF}} = 0$. The voltages should be devided with a factor of $\epsilon_2 = 0.625$ to get the most efficient acceleration of the beam. If the accelerator is driven with the lower beam currents used until now, 50 % of the RF-power can be saved. A enhancement of the synchrotron frequency is possible but only reasonable for the storage mode. At least the phase stability of the second RF station should be below 1.1° to prevent reflections at injection energy.

APPENDIX A

Appendix

A.1 Efficiency simulation plots

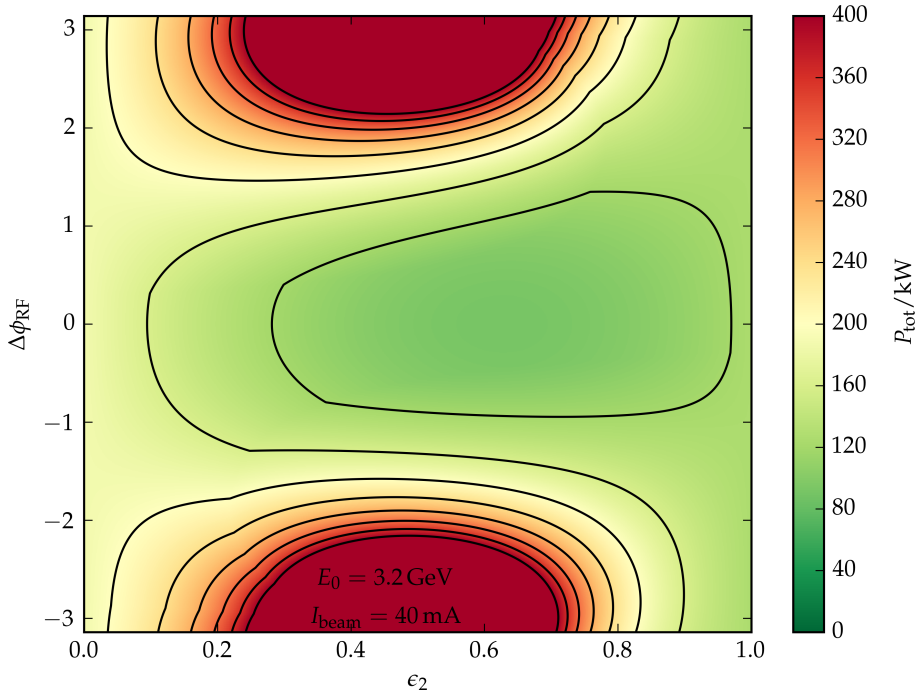

Figure A.1 – Total klystron power needed to accelerate a 40 mA beam at 3.2 GeV.

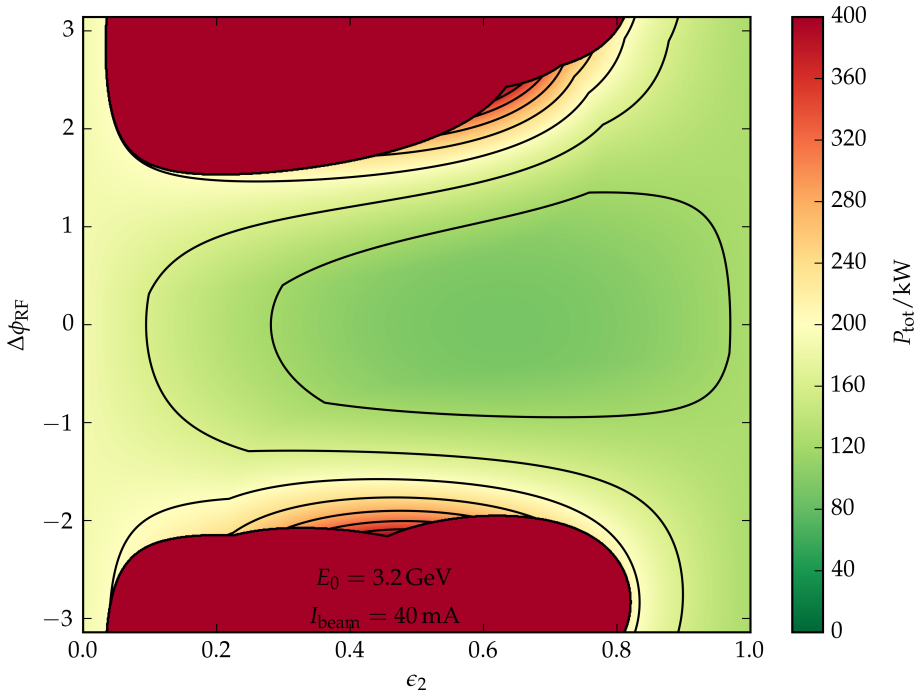

Figure A.2 – Total klystronpower needed to accelerate a 40 mA beam at 3.2 GeV. In the deep red regions the needed power at at least one klystron would be higher than 200 kW

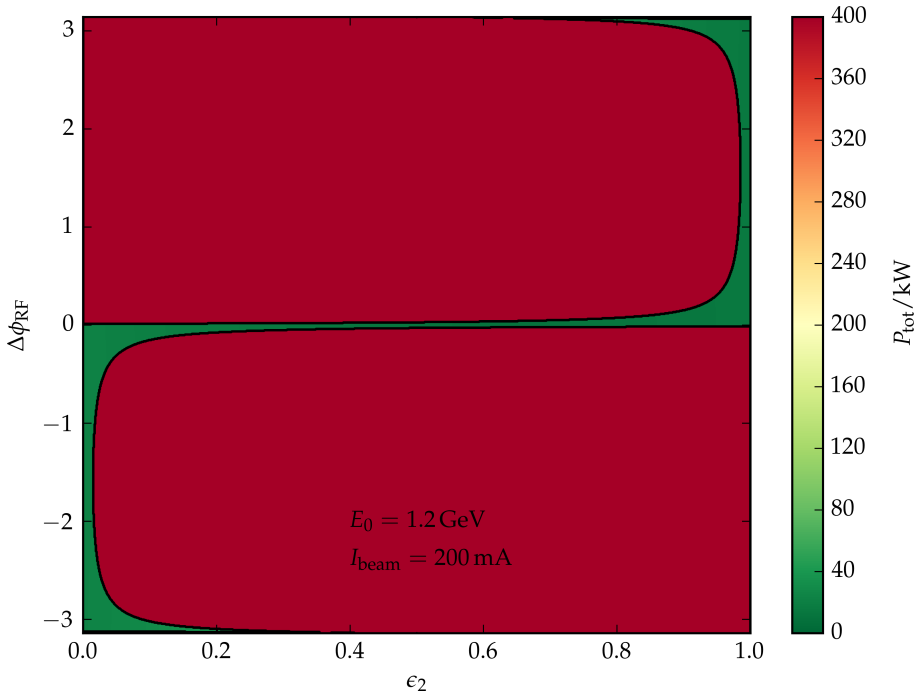

Figure A.3 – Possible operation parameters of ϵ_2 and $\Delta\phi_{\mathrm{RF}}$ at injection energy of 1.2 GeV and a beam current of 200 mA

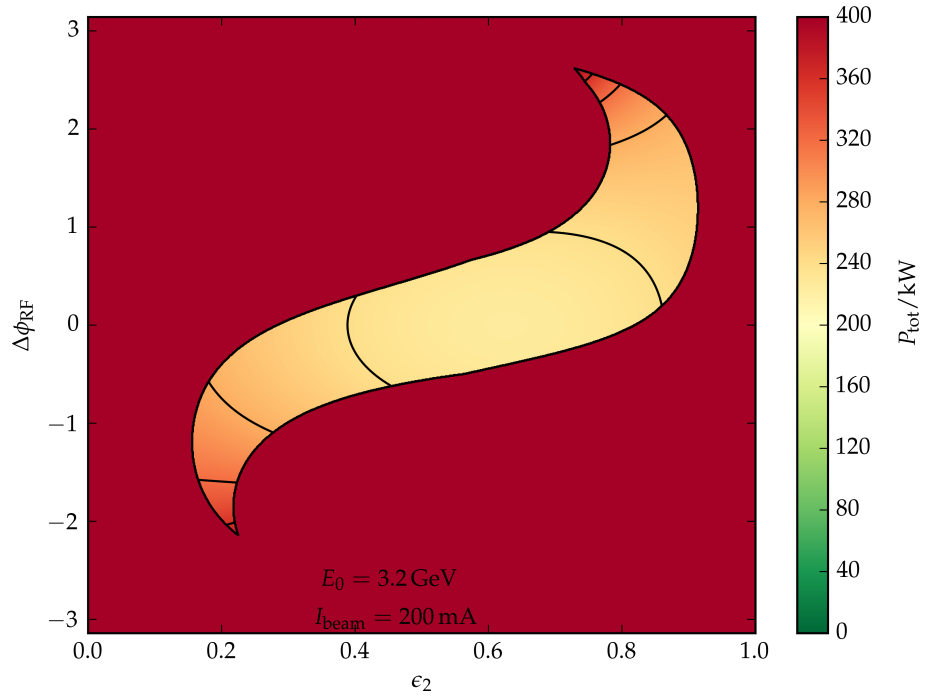

Figure A.4 – Acceptable operational region at an energy of 3.2 GeV for an beam current of 200 mA with excluded regions of reflections and technically not possible beam storage

A.2 Mathematical derivations

A.2.1 Free field wave equations

The Maxwell equations can be written as [Jac75]:

$$\vec{\nabla} \cdot \vec{E} = \frac{\rho}{\varepsilon_0} \tag{M1}$$

$$\vec{\nabla} \times \vec{E} = -\frac{\partial \vec{B}}{\partial t} \tag{M2}$$

$$\vec{\nabla} \cdot \vec{B} = 0 \tag{M3}$$

$$\vec{\nabla} \times \vec{B} = \mu_0 \vec{j} + \mu_0 \varepsilon_0 \frac{\partial \vec{E}}{\partial t} \tag{M4}$$

To obtain the wave equations one applies the rotation on M2 and M4:

$$\vec{\nabla} \times \left(\vec{\nabla} \times \vec{E}\right) = \vec{\nabla} \times \left(-\frac{\partial}{\partial t}\vec{B}\right)$$

$$\Rightarrow \vec{\nabla} \underbrace{\left(\vec{\nabla} \cdot \vec{E}\right)}_{=\frac{\rho}{\varepsilon_0}=0} - \Delta\vec{E} = -\frac{\partial}{\partial t}\left(\vec{\nabla} \times \vec{B}\right)$$

$$\Rightarrow -\Delta\vec{E} = -\frac{\partial}{\partial t}\left(\underbrace{\mu_0 \vec{j}}_{=0} + \underbrace{\mu_0\varepsilon_0}_{1/c^2}\frac{\partial}{\partial t}\vec{E}\right)$$

$$\Rightarrow \Delta\vec{E} = \frac{1}{c^2}\frac{\partial^2\vec{E}}{\partial t^2}$$

ρ and $\vec{j}$ are equal to zero since we want do derive the free field wave equations, what means that there are no charges or currents. One obtains the waveequation for the $\vec{E}$-field:

$$\Rightarrow \Delta\vec{E} - \frac{1}{c^2}\frac{\partial^2\vec{E}}{\partial t^2} = 0 \tag{A.1}$$

Similarly one gets the equation for the $\vec{B}$-field:

$$\vec{\nabla} \times \left(\vec{\nabla} \times \vec{B}\right) = \underbrace{\mu_0 \vec{j}}_{=0} + \underbrace{\mu_0\varepsilon_0}_{1/c^2}\frac{\partial}{\partial t}\vec{E}$$

$$\Rightarrow \vec{\nabla} \underbrace{\left(\vec{\nabla} \cdot \vec{B}\right)}_{=0} - \Delta\vec{B} = \vec{\nabla} \times \left(\frac{1}{c^2}\frac{\partial}{\partial t}\vec{E}\right)$$

$$\Rightarrow -\Delta\vec{B} = \frac{1}{c^2}\frac{\partial}{\partial t}\left(\vec{\nabla} \times \vec{E}\right)$$

$$\overset{M2}{=} \frac{1}{c^2}\frac{\partial}{\partial t}\left(-\frac{\partial}{\partial t}\vec{B}\right)$$

$$\Rightarrow \Delta\vec{B} = \frac{1}{c^2}\frac{\partial^2\vec{B}}{\partial t^2}$$

The wave equation for the $\vec{B}$-field writes:

$$\Delta\vec{B} - \frac{1}{c^2}\frac{\partial^2\vec{B}}{\partial t^2} = 0 \tag{A.2}$$

A.2.2 Modes in cylindrical cavities

Solving the wave equations A.1 and A.2 for the boundary conditions of a cylindrical so called pillbox cavity with radius R and length L using cylindrical coordinates (r,φ and z) with the Laplace operator in cylindrical coordinates:

$$\Delta f = \frac{1}{r}\frac{\partial}{\partial r}\left(r\frac{\partial f}{\partial r}\right) + \frac{1}{r^2}\frac{\partial^2 f}{\partial \varphi^2} + \frac{\partial^2 f}{\partial z^2} \tag{A.3}$$

One gets the following solutions for the different field distributions in the cavity. The solutions are divided in two blocks, the transversal magnetic TM modes which have no magnetic fields in longitudinal direction $B_z = 0$ and the transversal electric TE which have no longitudinal electric field $E_z = 0$. For the TM_{mnp} modes one gets [Wan04]:

$$E_z = E_0 J_m\left(\frac{x_{mn} r}{R}\right)\cos(m\varphi)\cos\left(\frac{p\pi z}{L}\right)e^{i\omega_{mnp}t} \tag{A.4}$$

$$E_r = -\frac{p\pi}{L}\frac{a}{x_{mn}} E_0 J'_m\left(\frac{x_{mn} r}{R}\right)\cos(m\varphi)\sin\left(\frac{p\pi z}{L}\right)e^{i\omega_{mnp}t} \tag{A.5}$$

$$E_\varphi = -\frac{p\pi}{L}\frac{ma^2}{x_{mn}^2 r} E_0 J_m\left(\frac{x_{mn} r}{R}\right)\sin(m\varphi)\sin\left(\frac{p\pi z}{L}\right)e^{i\omega_{mnp}t} \tag{A.6}$$

$$B_z = 0 \tag{A.7}$$

$$B_r = -i\omega_{mnp}\frac{ma^2}{x_{mn}^2 r c^2} E_0 J_m\left(\frac{x_{mn} r}{R}\right)\sin(m\varphi)\cos\left(\frac{p\pi z}{L}\right)e^{i\omega_{mnp}t} \tag{A.8}$$

$$B_\varphi = -i\omega_{mnp}\frac{a}{x_{mn} c^2} E_0 J'_m\left(\frac{x_{mn} r}{R}\right)\cos(m\varphi)\cos\left(\frac{p\pi z}{L}\right)e^{i\omega_{mnp}t} \tag{A.9}$$

The TE_{mnp} modes can be expressed as follows:

$$B_z = B_0 J_m\left(\frac{x_{mn} r}{R}\right)\cos(m\varphi)\sin\left(\frac{p\pi z}{L}\right)e^{i\omega'_{mnp}t} \tag{A.10}$$

$$B_r = \frac{p\pi}{L}\frac{a}{x'_{mn}} B_0 J_m\left(\frac{x_{mn} r}{R}\right)\cos(m\varphi)\cos\left(\frac{p\pi z}{L}\right)e^{i\omega'_{mnp}t} \tag{A.11}$$

$$B_\varphi = -\frac{p\pi}{L}\frac{ma^2}{x'^2_{mn} r} B_0 J_m\left(\frac{x_{mn} r}{R}\right)\sin(m\varphi)\cos\left(\frac{p\pi z}{L}\right)e^{i\omega'_{mnp}t} \tag{A.12}$$

$$E_z = 0 \tag{A.13}$$

$$E_r = i\omega'_{mnp}\frac{ma^2}{x'^2_{mn} r} B_0 J_m\left(\frac{x_{mn} r}{R}\right)\sin(m\varphi)\sin\left(\frac{p\pi z}{L}\right)e^{i\omega'_{mnp}t} \tag{A.14}$$

$$E_\varphi = i\omega'_{mnp}\frac{a}{x'_{mn}} B_0 J'_m\left(\frac{x_{mn} r}{R}\right)\cos(m\varphi)\sin\left(\frac{p\pi z}{L}\right)e^{i\omega'_{mnp}t} \tag{A.15}$$

A.2.3 Longitudinal beam dynamics

To describe the synchrotron oscillations around the reference phase one starts with the phase shift per revolution $(\Delta\phi)_{\mathrm{rev}}$ (derivation based on [Wil92]).

$$(\Delta\phi)_{\mathrm{rev}} = \omega_{\mathrm{RF}} \cdot \Delta T = h\omega_0 \cdot \Delta T = -h\omega_0 \eta T_0 \frac{\Delta p}{p_0} = -2\pi h\eta\frac{\Delta p}{p_0} \tag{A.16}$$

The harmonic number of ELSA is $h = {}^{\omega_{\mathrm{RF}}}/_{\omega_0} = 274$ this means that one bunch of particles needs h oscillations of the RF-field to travel one turn in the accelerator and it is possible to store h bunches in the accelerator.

Energy and momentum are connected via the relativistic energy momentum relation $E^2 = m^2c^4 + p^2c^2$ this leads a factor of β^2 for the connection of relative energy and momentum deviation.

$$\frac{\Delta E}{E_0} = \beta^2\frac{\Delta p}{p_0} \tag{A.17}$$

Now one can express the phase deviation per turn as:

$$(\Delta\phi)_{\text{rev}} = -\frac{2\pi h\eta}{\beta^2}\frac{\Delta E}{E_0} \tag{A.18}$$

To get the change of the phase deviation one can divide the deviation per turn by the time a particle needs for one revolution.

$$\frac{\mathrm{d}}{\mathrm{d}t}\Delta\phi = \frac{(\Delta\phi)_{\text{rev}}}{T_0} \overset{A.18}{=} -\frac{2\pi h\eta}{\beta^2 T_0 E_0}\Delta E \tag{A.19}$$

The total energy change of a particle per turn is than the difference between gained energy due to acceleration ΔE_{kin} (equation 2.2) in the cavities and energy loss due to synchrotron radiation $W(E) = \Delta E_{\text{rev}}(E)$.

$$(\Delta E)_{\text{rev}} = \Delta E_{\text{kin}} - W(E) \overset{2.2}{=} eU(\phi) - W(E) \tag{A.20}$$

Because of small deviations from reference phase and energy one can use Taylor expansions.

$$(\Delta E)_{\text{rev}} \approx eU(\phi_0) + e\left.\frac{\mathrm{d}U(\phi)}{\mathrm{d}\phi}\right|_{\phi=\phi_0}\Delta\phi - \left(W(E_0) + \left.\frac{\mathrm{d}W(E)}{\mathrm{d}E}\right|_{E=E_0}\Delta E\right) \tag{A.21}$$

Since $eU(\phi_0) - W(E_0)$ is zero because the accelerating voltage on the reference phase should compensate the synchrotron losses exactly (equation 2.29), the energy change per turn gets:

$$(\Delta E)_{\text{rev}} = e\cdot\underbrace{\left.\frac{\mathrm{d}U(\phi)}{\mathrm{d}\phi}\right|_{\phi=\phi_0}}_{U_0\cos(\phi_0)}\Delta\phi - \left.\frac{\mathrm{d}W(E)}{\mathrm{d}E}\right|_{E=E_0}\Delta E \tag{A.22}$$

The derivative of the energy deviation can be calculated if equation A.22 is divided by revolution time T_0.

$$\frac{\mathrm{d}}{\mathrm{d}t}\Delta E = \frac{(\Delta E)_{\text{rev}}}{T_0} = \frac{e}{T_0}\cdot U_0\cos(\phi_0)\Delta\phi - \left.\frac{\mathrm{d}W(E)}{\mathrm{d}E}\right|_{E=E_0}\Delta E \tag{A.23}$$

To get the equation for oscillation in $\Delta\phi$ one derives equation A.19 with respect to time and puts in equation A.23.

$$\frac{\mathrm{d}^2}{\mathrm{d}t^2}\Delta\phi = -\frac{2\pi h\eta}{\beta^2 T_0 E_0}\frac{\mathrm{d}}{\mathrm{d}t}\Delta E \tag{A.24}$$

One receives the oscillation equation:

$$\frac{\mathrm{d}^2\Delta\phi}{\mathrm{d}t^2} + 2\alpha_s\frac{\mathrm{d}\Delta\phi}{\mathrm{d}t} + \Omega_s^2\Delta\phi = 0 \tag{A.25}$$

With synchrotron frequency Ω_s and damping of the synchrotron motion α_s:

$$\Omega_s = \sqrt{\frac{2\pi h\eta e}{\beta^2 T_0^2 E_0} U_0 \cos(\phi_0)} \tag{A.26}$$

$$\alpha_s = \frac{1}{2T_0} \left.\frac{\mathrm{d}W(E)}{\mathrm{d}E}\right|_{E=E_0} \tag{A.27}$$

A.2.4 Large amplitude oscillations

To get the form of the RF-potential in which the particles oscillate one has to evaluate the motion of the particles with larger amplitude $\Delta\phi$ and therefore their phase passing the cavity $\phi = \phi_0 + \Delta\phi$. Therefore we have another look on the derivative of equation A.20 and expand only the $W(E)$ term. With $W(E_0) = eU_{\mathrm{rev}}$ one gets:

$$\frac{\mathrm{d}}{\mathrm{d}t}\Delta E = \frac{e}{T_0} \cdot \Big(U_0 \sin(\phi_0 + \Delta\phi) - \underbrace{U_0 \sin(\phi_0)}_{U_{\mathrm{rev}}}\Big) - \underbrace{\left.\frac{\mathrm{d}W(E)}{\mathrm{d}E}\right|_{E=E_0} \frac{\Delta E}{T_0}}_{\approx 0} \tag{A.28}$$

By multiplication of A.19 and A.28 one gets:

$$-\frac{\pi h\eta}{\beta^2 T_0 E_0} \underbrace{2\Delta E \frac{\mathrm{d}}{\mathrm{d}t}(\Delta E)}_{\frac{\mathrm{d}}{\mathrm{d}t}(\Delta E)^2} = \frac{e}{T_0} U_0 \Bigg(\underbrace{\frac{\mathrm{d}}{\mathrm{d}t}(\Delta\phi)\sin(\phi_0 + \Delta\phi)}_{-\frac{\mathrm{d}}{\mathrm{d}t}\cos(\phi_0+\Delta\phi)} - \frac{\mathrm{d}}{\mathrm{d}t}(\Delta\phi)\sin(\phi_0)\Bigg) \tag{A.29}$$

Putting everything together:

$$\frac{\mathrm{d}}{\mathrm{d}t}(\Delta E)^2 = \frac{\mathrm{d}}{\mathrm{d}t}\frac{e\beta^2 E_0}{\pi h\eta} U_0 \Big(\cos(\phi_0 + \Delta\phi) + \Delta\phi \sin(\phi_0)\Big) \tag{A.30}$$

Integrating this equation one gets an additional constant C.

$$\Rightarrow (\Delta E)^2 = \frac{e\beta^2 E_0}{\pi h\eta} U_0 \Big(\cos(\phi_0 + \Delta\phi) + \Delta\phi \sin(\phi_0)\Big) + C \tag{A.31}$$

$$\Rightarrow (\Delta E)^2 - \frac{e\beta^2 E_0}{\pi h\eta} U_0 \Big(\cos(\phi_0 + \Delta\phi) + \Delta\phi \sin(\phi_0)\Big) = C \tag{A.32}$$

$$\Rightarrow (\Delta E)^2 + V(\Delta\phi) = C \tag{A.33}$$

Therefore the potential can be written as:

$$V(\Delta\phi) = -\frac{e\beta^2 E_0}{\pi h\eta} U_0 \Big(\cos(\phi_0 + \Delta\phi) + \Delta\phi \sin(\phi_0)\Big) \tag{A.34}$$

Bibliography

[15] *Procceedings of IPAC2015*, Richmond, USA, 2015.

[Hil06a] W. Hillert, *The Bonn Electron Strecher Accelerator ELSA: Past and future*, The European Physical Journal A **28** (2006).

[Die+15] F. Dietz et al., *Photoproduction of ω mesons off protons and neutrons*, The European Physical Journal A **51** (2015).

[Sch] H. Schmieden, *BGO-OD Experiment - Meson photoproduction*, URL: `https://bgo-od.physik.uni-bonn.de/` (visited on 19/03/2016).

[Heu+13] N. Heurich et al., "A new external beamline for detector tests", *Procceedings of IPAC2013*, Shanghai, China, 2013.

[Heu11] N. Heurich, *Dämpfung von Strahlinstabilitäten im Elektronenbeschleuniger ELSA mithilfe von Breitbandresonatoren*, Bonn, 2011.

[Hil08] W. Hillert, "E106 Hohlraumresonatoren/Cavities: Details on the experimental method", Lab course information, 2008.

[Lee12] S. Lee, *Accelerator Physics*, Singapore: World Scientific, 2012.

[Sch15] M. Schelder, *Intensitäts- und Energieerhöhung an ELSA*, PhD thesis: Rheinische Friedrich-Wilhelms-Universität Bonn, 2015.

[Wil92] K. Wille, *Physik der Teilchenbeschleuniger und Synchrotronstrahlungsquellen*, Stuttgart: Teubner, 1992.

[Rot08] A. Roth, *Studien zum Einsatz supraleitender Hochfrequenzresonatoren für Energien bis 5 GeV an der Beschleunigeranlage ELSA*, Diploma thesis: Physikalisches Institut der Universität Bonn, 2008.

[Jac75] J. Jackson, *Classical electrodynamics*, Wiley, 1975, ISBN: 9780471431329.

[Wie93] H. Wiedemann, *Particle accelerator physics*, Springer, 1993.

[Sch+15a] J. F. Schmidt et al., "Measurement of momentum compaction factor via depolarizing resonances at ELSA", *Procceedings of IPAC2015*, Richmond, USA, 2015.

[Hil06b] W. Hillert, "Accelerator Physics I", lecture script, Bonn, Germany, Summer Term 2006.

[Sch+15b] M. Schedler et al., "A New RF station for the ELSA Stretcher Ring", *Procceedings of IPAC2015*, Richmond, USA, 2015.

[DES10] DESY-MHFe, *Data Sheet 500MHz, 5-Cell Cavity*, 2.0, Hamburg, Germany, 2010, URL: `https://mhf-e.desy.de/e5/e63/` (visited on 21/03/2016).

[Tho81] Thomson-CSF, *F2055 High-Power Klystron*, Boulogne-Billancourt Cedex, France, 1981, URL: `https://mhf-e.desy.de/e5/e73/` (visited on 22/03/2016).

[DES05] DESY-MHFe, *Data Sheet: Rechteck-Hohlleiter (allgemein)*, Vers. 1.0, Hamburg, Germany, 2005, URL: https://mhf-e.desy.de/e5/e35/ (visited on 22/03/2016).

[DESa] DESY-MHFe, *Overview drawing of input coupler and the waveguide transition*, Hamburg, Germany, URL: https://mhf-e.desy.de/e5/e63/ (visited on 22/03/2016).

[DES11] DESY-MHFe, *Data Sheet: Cavity Input Coupler*, Vers. 1.3, Hamburg, Germany, 2011, URL: https://mhf-e.desy.de/e5/e63/ (visited on 22/03/2016).

[DES15] DESY-MHFe, *Data Sheet 500MHz, 7-Cell Cavity*, 3.2, Hamburg, Germany, 2015, URL: https://mhf-e.desy.de/e5/e63/ (visited on 21/03/2016).

[DESb] DESY-MHFe, *Data Sheet: Cavity Tuning PLunger (Feinabstimmung)*, Vers. 3.0, Hamburg, Germany, URL: https://mhf-e.desy.de/e5/e63/ (visited on 22/03/2016).

[Sau13] D. Sauerland, *Amplituden-, Phasen- und Temperaturstabilisierung des Hochfrequenzsystems an ELSA*, Bonn, 2013.

[Deu15] C. Deutsch, *Störkörpermessung an Hohlraumresonatoren*, Physikalisches Institut der Universität Bonn, 2015.

[Tey] D. Teytelman, URL: http://dimtel.com/.

[Wan04] T. P. Wangler, *RF Linear Accelerators*, Wiley Series in Beam Physics and Accelerator Technology, Weinheim: WILEY-VCH Verlag GmbH & Co. KGaA, 2004.

List of Figures

2.1 Sketch of a thermionic electron gun . . . 3
2.2 RF acceleration of a bunched electron beam . . . 4
2.3 Coordinate system used to describe cylindrical resonators [Heu11] . . . 5
2.4 Simulation of the E (left) and B field (right) of the TM_{010} mode in a pillbox cavity simulated with *CST Microwave studio*. The higher the field strength the bigger the arrows. Additionally higher field strength are shown in red lower in yellow. [Hil08] . . . 6
2.5 Simulation of the electric field of the TM_{010} mode in a seven cell PETRA type cavity. The higher the fieldstregth the bigger the arrows (for high fieldstrength yellow/orange and lower blue). The nosecones which enhance the fieldstrength on the beam axis can be seen, too. Fields are calculated numerically with *CST Microwave Studio* . . . 6
2.6 Equivalent circuit of a cavity with RF generator and coupling [Sch15] . . . 7
2.7 Wave progatation of the TE_{10}-mode through a WR1800 waveguide simulated with *CST Microwave studio*. The electric field strength is depicted. Higher field strength are red, lower blue. The picture is a snapshot of the fields. The 500 MHz wave is injected at the left end of the waveguide and propagates to the other end. The right end of the waveguide simulates an matched termination, that the waves are not reflected back in the waveguide. 9
2.8 Electric fields of the TE_{10} mode with a frequency of 500 MHz in a magic T with RF power injected from the top and the fourth port in the front terminated with the impedance of the waveguide. Higher field strength are depicted in red, lower in blue.The fields are calculated with *CST Microwave studio.* . . . 10
2.9 Scheme of a circulator . . . 11
2.10 Working principle of a klystron [Hil06a]. . . . 11
2.11 Scheme of a circularly shaped synchrotron. The dipole magnets bending the beam on a circular path are shown in green. The RF-section is depicted in pink. . . . 12
2.12 Principle of phase focusing in an elliptical accelerator [Sch15] . . . 13
2.13 Acceleration voltage and potential dependent on phase ϕ of the accelerating voltage [Sch15]. 14
2.14 Sketch of a C-shaped electric dipole magnet [Hil06b]. . . . 15
2.15 Sketch of a quadrupole magnet, the hyperbolic shaped poles are orange. The magnetic field lines are depicted in green, while the forces on two particles with different positions on the quadrupole are shown in red. [Hil06b]. . . . 16

3.1 ELSA floorplan . . . 20
3.2 Beam current and energy in the boostermode of ELSA [Sch+15b] . . . 21
3.3 Photograph of one PETRA five cell cavity in the existing RF station. . . . 21
3.4 Position of the new cavities in the stretcherring (red ellipse) and site of the new klystron (orange) . . . 22
3.5 Photograph of a PETRA seven cell cavity. [DES15] . . . 23
3.6 Scheme of the cooling for the RF resonators [Sch15] . . . 24

3.7 Setup for a bead pull measurement of a PETRA seven cell cavity [Deu15] 24
3.8 Photoraph of a coupling loop for PETRA type cavities 26
3.9 So called CERN-Coupler with fitting coupling loop. 26
3.10 Absolute fieldstrength of the electric field in a cornered waveguide simulated with *CST Microwave studio*. High field strength are depicted in red lower in blue. 27
3.11 Planed setup for the waveguide transition of the new RF-station. (P. Hänisch) 27
3.12 Components of the second RF-station in the ELSA tunnel. (P. Hänisch) 28
3.13 Klystron site with high voltage power supply on the left site and klystron on the right. The rectangular incoupling in the WR1800 waveguide can be seen on the right site of the klystron. 29
3.14 Cirulator for WR1800 waveguides. The Forward power comes from the left and is transmitted to the right. Reflected power from the right is damped in the watercooled load in the front. 29
3.15 Schematic setup of the LLRF-system which will be used ad the second RF-station. [Sch+15b] 30

4.1 Input and output data of the software `hfplotter.py` and processing of these data . . . 33
4.2 Voltages of the two RF-Stations for typical parameters and no phase difference between the two stations 34
4.3 Graphical user interface for the calculation of the voltages in both stations. In the left plot the RF-Potential and in the right the voltages of both stations (red,blue) and the resulting total voltage (purple) can be seen. The main input parameters for the calculation can be adjusted by the sliders. 35
4.4 Powers P_1 and P_2 which the two klystrons of the stations have to generate to accelerate a 40 mA beam current at an energy of 3.2 GeV with $\Delta\phi_{\mathrm{RF}} = 0$. P_{tot} is the sum of the powers of both stations. 35
4.5 Storable beam current in ELSA at an energy of 3.2 GeV with no phase difference between the two RF-stations. Technically not operatable regions are marked in deep red. 36
4.6 Klystron power for a beam current of 200 mA depending on the synchrotron frequency f_{s} and the beam energy E_0. Technically not operatable regions are marked in deep red. 37
4.7 Beam lifetime χ_s of beams with different synchrotron frequencies f_s depending on their energy E_0 [Sch15] 37
4.8 Acceptable parameters at injection energy 38
4.9 Accelerating voltages with phase difference chosen in a way that in station one the beam loading vanishes. This means the acceleration voltage on the reference phase is zero in station one 39
4.10 Total klystron power needed to accelerate a 40 mA beam at 3.2 GeV. Plots without these exclusions can be found in the appendix. 40
4.11 Needed power of the klystrons with a phase difference of both stations of $\Delta\phi_{\mathrm{RF}} = -0.45$. 40
4.12 Negative reference voltage in one RF-station. 41

A.1 Total klystron power needed to accelerate a 40 mA beam at 3.2 GeV. 43
A.2 Total klystronpower needed to accelerate a 40 mA beam at 3.2 GeV. In the deep red regions the needed power at at least one klystron would be higher than 200 kW 44
A.3 Possible operation parameters of ϵ_2 and $\Delta\phi_{\mathrm{RF}}$ at injection energy of 1.2 GeV and a beam current of 200 mA 44
A.4 Acceptable operational region at an energy of 3.2 GeV for an beam current of 200 mA with excluded regions of reflections and technically not possible beam storage 45

List of Tables

3.1 Parameters of PETRA five cell cavities as specified in the data sheet [DES10] 19
3.2 Most important parameters of PETRA seven cell cavities as specified in the data sheet [DES15] 23

4.1 Input and output parameters of the software `hfplotter` 33
4.2 Optimum operation parameters for two RF stations 36
4.3 Optimum coupling factors for different beam currents and energies for the new cavities at ϵ_2^{opt} 41

Glossary

BGO-OD Experiment for hadron spectroscopy. Main calorimeter made of BGO ($Bi_4Ge_3O_{12}$) crystals. Another important part of the experiment is a hugh dipole magnet the open dipole OD. 2, 19

CBELSA Experiment for hadron spectroscopy. The main calorimeter is shaped like a barrel and made out of crystals therefore the experiment is called crystal barrel CB located at the accelerator facility ELSA. 2, 19

DESY Deutsches Elektronen-SYnchrotron, german for german electron synchrotron, research centre for accelerator physics located in Hamburg. 19

FODO magnetic structure of an accelerator: Focusing quadrupole F - O as 0 for driftspace without quadrupole - Defocusing Quadrupole D - O for driftspace . 17

LLRF The low level radio frequency system is the which controls output phase and amplitude of a klystron in a particle accelerator. 22, 29, 30, 34, 38, 39, 54

Acronyms

ELSA electron stretcher accelerator. 1, 2, 13, 14, 17, 19, 21, 26, 28, 36, 47, 53, 54

LINAC linear accelerator. 2, 19

PETRA positron electron tandem ring accelerator. 6, 7, 19, 21–26, 53, 54, 57

PS power supply. 11

QCD quantum chromo dynamics. 2

RF radio frequency. iii, 1, 3–5, 7, 10–12, 14, 19, 21–34, 36–38, 40, 41, 47, 49, 53, 54, 57

Acknowledgements

Gratitude has to be owed to everyone who accompanied me on my way through the formation of this thesis.

PD Dr. Wolfgang Hillert for beeing my supervisor and introducing me into this interesting topic. The door to his office was always open if an good advice was needed or unconventional questions came up.

I would like to thank Prof. Dr. Klaus Desch for becoming the second referee and taking some time to evaluate my thesis.

My great appreciation goes to Philipp Hänisch supporting me in learning some engineering tools.

Special thanks I would like to offer to everyone at ELSA, Dennis Sauerland, Jens-Peter Thiry, Dennis Proft and Jan Schmidt for the discussions about RF problems, the help in solving software problems and the reading of unready versions of my thesis and giving me lots of useful tips to improve it.

Rebecca Koop, Nikolas Heurich, Michael Switka, Florian Hinterkeuser, Dr. Andreas Diekmann and Dr. Frank Frommberger for a lot of useful and inspiring conversations and taking me as a part of ELSA.

Christopher Deutsch and Manuel Schedler for the short but intense time in the common office.

Sandra and Verena Unruh for keeping the timeslots free for me to work on the thesis.

The office RF station for providing me with lots of unhealthy food.

And at least Heinz und Christa Derksen for their comprehensive encouragement while the whole time of my studies.

Thanks.